Modelling groundwater recharge, actual evaporation and transpiration in semi-arid sites of the Lake Chad Basin: The role of soil and vegetation on groundwater recharge

Christoph Neukum[1], Angela Gabriela Morales Santos[2], Melanie Ronelngar[3], Aminu Bala[4], Sara Ines Vassolo[1]

[1] Federal Institute for Geosciences and Natural Resources, Department of Groundwater and Soil, Stilleweg 2, 30655 Hannover, Germany
[2] University of Natural Resources and Life Sciences, Vienna, Department of Water, Atmosphere and Environment, Institute for Soil Physics and Rural Water Management, Muthgasse 18, 1190 Vienna, Austria
[3] Federal Institute for Geosciences and Natural Resources at Lake Chad Basin Commission, Rond Point des Armes, Ndjamena, Chad
[4] Lake Chad Basin Commission, Rond Point des Armes, Ndjamena, Chad

Correspondence to: Christoph Neukum (christoph.neukum@bgr.de)

Abstract

The Lake Chad Basin, located in the center of North Africa, is characterized by strong climate seasonality with a pronounced short annual precipitation period and high potential evapotranspiration. Groundwater is an essential source for drinking water supply as well as for agriculture and groundwater related ecosystems. Thus, assessment of groundwater recharge is very important although difficult, because of the strong effects of evaporation and transpiration as well as limited available data.

A simple, generalized approach, which requires only limited field data, freely available remote sensing data as well as well-established concepts and models, is tested for assessing groundwater recharge in the southern part of the basin. This work uses the FAO-dual K_c concept to estimate E and T coefficients at six locations that differ in soil texture, climate, and vegetation conditions. Measured values of soil water content and chloride concentrations along vertical soil profiles together with different scenarios for E and T partitioning and a Bayesian calibration approach are used to numerically simulate water flow and chloride transport using Hydrus-1D. Average groundwater recharge rates and the associated model uncertainty at the six locations are assessed for the 2003-2016 time-period.

Annual groundwater recharge varies between 6 and 93 mm and depends strongly on soil texture and related water retention and on vegetation. Interannual variability of groundwater recharge is generally greater than the uncertainty of the simulated groundwater recharge.

1 Introduction

Recharge occurs even in the most arid regions, mainly due to concentration of surface flow and ponding with lateral and vertical infiltration (Lloyd, 1986). Direct recharge by precipitation is possible in semi-arid regions, but intermittently, owing to the fluctuations in the periodicity and volume of precipitation that is inherent to such regions (Lloyd, 2009). Scanlon et al.

(2006) synthesized recharge estimates for semiarid and arid regions worldwide. They found that recharge is sensitive to land use and cover changes, hence management of such changes are necessary to control recharge. Moreover, they stated that average recharge rates in semi-arid and arid regions range from 0.2 to 35 mm yr^{-1}, representing 0.1 to 5% of long-term average annual precipitation. Recently, Cuthbert et al. (2019) investigated the relationship between precipitation and recharge in sub-Saharan Africa using multidecadal hydrographs. They found that focused recharge predominates in arid areas and is mainly controlled by intense rainfall and flooding events. Intense precipitation, even during years of low annual precipitation, results in some of the most significant years of recharge in dry subtropical locations.

The arid to semi-arid Lake Chad Basin (LCB) is one of the largest endorheic basins of the world with an area of approximately 2.5 million km^2. It covers parts of Algeria, Cameroon, Central African Republic, Chad, Libya, Niger, Nigeria, and Sudan. According to the Lake Chad Basin Commission (LCBC, 2012), 45 million inhabitants are settled in the basin. The study areas of Salamat and Waza Logone are located in the southern part of the LCB along the Chari-Logone, the major tributary river system to Lake Chad (Figure 1), which accounts for around 80-90% of the inflow to the Lake Chad (Bouchez et al., 2016).

Groundwater is an important source for drinking water supply as well as for agriculture and groundwater related ecosystems in the LCB. Lake Chad, associated rivers, and the floodplains of the major rivers are characterized by strong seasonality, due to a pronounced short annual precipitation period and high potential evapotranspiration. Groundwater recharge, evaporation, transpiration, and the entire hydrological budget depend strongly on seasonality. However, the impact of transpiration as a potentially significant process of the hydrological budget (Jasechko et al., 2013) has not yet been intensively explored in the region (Bouchez et al., 2016).

Many studies have been published concerning the hydrological behaviour and budget of Lake Chad, due to its substantial and frequent open water surface changes and related consequences to the population and the environment (e.g. Bouchez et al., 2016; Lemoalle et al., 2014; Lemoalle et al., 2012; Olivry et al., 1996; Vuillaume, 1981). Another important topic associated to Lake Chad is groundwater recharge by infiltration of lake water into the Quaternary aquifer, which was estimated by isotope studies (Fontes et al., 1969; Fontes et al., 1970; Zairi, 2008), water and salt budgets (Bouchez et al., 2016; Bader et al., 2011; Carmouze, 1972; Roche, 1980), and hydrogeological models (Isihoro et al., 1996; Leblanc, 2002).

Very significant for an arid to semi-arid region is the determination of diffuse groundwater recharge, evaporation of surface and soil water as well as transpiration from plants. In the LCB, recharge has been assessed using different methods. The Chloride Mass Balance (CMB) approach is a widely used technique. Edmunds and Gaye (1994) used interstitial water chloride profiles from the unsaturated zone, in combination with measurements of chemical parameters from dug well samples, to calculate groundwater recharge in the Sahel. They estimated a recharge rate of 13 mm $year^{-1}$ for a mean annual rainfall from 1970-1990 at 280 mm in their study area and concluded that it is an inexpensive technique, which can be applied in many arid and semi-arid areas. Applying the same method, Edmunds et al. (2002) estimated direct recharge rates from precipitation in the Manga Grasslands in NE Nigeria (western LCB) at rates between 16 mm $year^{-1}$ and 30 mm yr^{-1}. Including Cl values from dug-wells, they appraised the regional direct recharge for north Nigeria at 43 mm $year^{-1}$, which highlights the importance of infiltration from precipitation to the groundwater table at the regional scale. Tewolde et al. (2019) applied the CMB on soil

profiles of the LCB, which are partly used in this study. They estimated generally lower annual recharge in Salamat (3 to 111 mm $year^{-1}$) compared to Waza Logone (117 to 163 mm $year^{-1}$), whereas very low values were found for Bahr el Ghazal (0.2 to 0.8 mm $year^{-1}$) and the northern pool of the Lake Chad (0.6 to 0.8 mm $year^{-1}$). They conclude that one major difficulty of CMB is the choice of a representative chloride concentration, or the concentration that prevails at greater depths, when evapotranspiration effects are negligible, particularly for soils with a strong vertical variability in chloride concentrations. Recharge has also been assessed using groundwater modelling in the LCB (Eberschweiler, 1993; Massuel, 2001; Leblanc, 2002; Boronina et al., 2005; Vaquero et al., 2021), where diffused recharge has been obtained in the process of model calibration. Calculated values differ considerably, depending on the vertical accuracy of the model and the extension of the modelled area. It is also possible to determine recharge with the help of isotopes. Goni et al. (2021) used environmental isotopes to conclude that recharge in the southwestern part of the LCB is mainly the result of strong precipitation events in the middle of the wet season. Using the Cl^{36} to Cl ratio, Bouchez et al. (2019) estimated a recharge rate of 240 ± 170 mm $year^{-1}$ for the humid part of the LCB in the south. Recharge rates reduce to 78 ± 7 mm $year^{-1}$ for areas close to surface water and to 16 ± 27 mm $year^{-1}$ for regions unconnected to the hydrological network in the Sahelian part.

Concerning evaporation and transpiration, they were assessed for the Lake Chad coupling hydrological, chemical, and isotopic models (Bouchez et al., 2016). They conclude, that evaporation varies from 2070 ± 100 mm $year^{-1}$ in the southern to 2270 ± 100 mm $year^{-1}$ in the northern pool, whereas transpiration is insignificant with an average of 300 mm $year^{-1}$ in the lake that increases slightly to 500 mm $year^{-1}$ in the archipielagos, where vegetation is abundant. Furthermore, they state that their work estimates transpiration of the Lake Chad for the first time. However, studies on evaporation and transpiration in the vadose zone are largely missing in the LCB.

For vadose zone studies, partitioning evapotranspiration (ET) into its respective soil evaporation (E) and plant transpiration (T) components is crucial for process-based understanding of fluxes (Anderson et al., 2017). There are a number of measurement and modelling approaches that can be used to estimate E and T separately, including micro-lysimeters, soil heat pulse probes, Bowen ratios, and Eddy covariance to determine E, and sap flow, chambers, and biomass-transpiration relationships to measure T (Kool et al., 2014). Evapotranspiration partitioning can also be estimated directly by using stable isotopes to assess the ratio between E and T (Wu et al. 2016). Stable isotopes were also used in combination with Eddy covariance on semi-arid environments (Aouade et al., 2016).

The Food and Agricultural Organization of the United Nations (FAO) published a model (Allen et al., 1998) that uses an empirically defined crop coefficient (K_c) in combination with a grass-reference potential ET (ET_0) to calculate crop potential evapotranspiration (ET_c). There are two approaches for this method: single coefficient and dual crop coefficient. The FAO-dual K_c model is a validated method for ET partitioning and the most commonly applied (Kool et al., 2014). It has been widely used with good results for numerous crops under different conditions: e.g. wheat and maize in semi-arid regions (Shahrokhnia and Sepaskhah, 2013), wheat in humid climates (Vieira et al., 2016), cherry trees in temperate continental monsoon climates (Tong et al., 2016), and irrigated eucalyptus (Alves et al., 2013) and canola in terrestrial climates (Majnooni-Heris et al., 2012).

Quantification of water fluxes in the vadose zone and linking atmospheric water and solute input at the upper boundary of the soil with water and solute fluxes at different soil depths is frequently implemented using different type of models. Numerical models need information on vadose zone properties for accurate parametrization to link fluxes with state variables such as unsaturated hydraulic conductivity and the water retention curve. Estimation of effective soil hydraulic parameters, which are valid at the modelling scale, might be laborious. Furthermore, parameter estimation might vary significantly depending on the measurement method (Mertens et al., 2005), when water and solute fluxes dynamics are considered. Hydraulic and transport parameters obtained from inverse modelling can be ambiguous, if multiple parameters are simultaneously considered and boundary conditions are not well known. Combining different state variables of water flow and solute transport in one objective function was found to be a useful strategy for appropriate parametrization (Groh et al., 2018; Sprenger et al., 2015) and for the transient simulation of water and solute fluxes. However, large amount of data are necessary to obtain accurate estimates of state variables, which are rarely available in remote areas of Africa, and measurement of related variables are associated with a huge effort in such environments. Pedotransfer functions (PTF) bridge available and needed data. They are frequently used to quantify soil parameters (van Looy et al., 2017; Vereecken et al., 2016). PTF strive to provide a balance between data accuracy and availability (Vereecken et al., 2016). Since PTF usually do not consider soil structure, their results are better for homogeneous soils than for structured ones (Sprenger et al., 2015; Vereecken et al., 2010).

In general, time series of relevant data for estimating groundwater recharge is scarce in the LCB. A simple, generalized approach, which requires only limited field data, freely available remote sensing data, and well-established concepts and models, is tested for assessing groundwater recharge in the semi-arid part of the LCB. This work applies the FAO-dual K_c concept to estimate E and T coefficients at six locations, which differ in soil texture, climate, and vegetation conditions. Measured values of soil water content and chloride concentrations along vertical soil profiles, partly published by Tewolde et al. (2019), together with different scenarios for E and T partitioning and a Bayesian calibration approach are used to numerically simulate water flow and chloride transport as well as to produce time series of recharge. Both measured soil-moisture and chloride concentrations are necessary for model calibration in order to get reliable estimates for water flow and solute transport. Average potential groundwater recharge and the associated model uncertainty are assessed for the 2003-2016 time-period. This generalized method is applied to selected sites for estimating recharge in areas with low accessibility, but cannot be extrapolated to the whole LCB.

2 Data and methods

2.1 Study sites

The LCB is a Mesozoic basin and a major part of its geology comprises sedimentary formations from the Tertiary and Quaternary periods (LCBC, 1993). The Quaternary sediments form a continuous layer of fluviatile, lacustrine and aeolian sands. These medium to fine-grained sands act as an unconfined transboundary aquifer, as do all aquifers in the LCB, and are isolated from underlying aquifers by a thick layer of Pliocene clay (Leblanc et al., 2007; Vassolo, 2009). The Tertiary formation

(Continental Terminal) consists of sandstones and argillaceous sands and is a classic example of a confined aquifer system that becomes artesian in the surroundings of Lake Chad (Ngatcha et al., 2008). The availability of water from precipitation as well as the deposition characteristics of the aquifer play an important role in the recharge of the upper unconfined sands (Vassolo, 2009).

The study sites (Figure 1, Table 1) are located in the Salamat and Waza Logone floodplains in the southern Sahel zone. Selection of sites was limited mainly by accessibility and project's goals. The sites correspond to those published by Tewolde et al. (2019) for these areas, except for site ST4. Site ST4 is located far from any floodplain, which is the focus of this research, and its soil composition and vegetation are very similar to those from site ST3. Thus, including this location would not provide any additional information.

The types of soils included in the selected sites are sand, loam, clay, and their combinations, which are the most common in the LCB. However, they surely do not cover all existent soils, due to the extension of the LCB. Sites ST1 and ST2 in Salamat as well as WL1 and WL3 in Waza Logone are annually flooded over three months, site WL2 located at the edge of the Waza Logone wetland is flooded only one month per year whereas site ST3, although close to ST1 in Salamat, is never flooded. In the Salamat region, mainly sorghum is grown with trees such as Acacia albida, A. scorpioides and A. sieberana, present along the margins of the floodplains (Bernacsek et al., 1992). In the Waza Logone area, vegetation depends on the duration of submersion, forming grass savannahs that are flooded for longer periods of time (Batello et al., 2004). The selected sites cover thus, the most common vegetation in the LCB. Acacia and grass are the most widespread natural vegetation, whereas sorghum is the most commonly planted corn. Cotton, which is also planted, is only locally produced and generally using irrigation. Mango trees can be found along the Chari and Logone rivers, but are not representative for the whole basin.

2.2 Climate data

Monthly precipitation and potential evapotranspiration data from 1970 to 2019 for the study sites were extracted from the CRUTS 4 database (Harris et al., 2020). The potential evapotranspiration was calculated using the Penman-Monteith method and is considered herein as the reference evapotranspiration (ET_0). Wind speeds at 10 m above ground for Salamat and Waza Logone were obtained from Didane et al. (2017). To adjust these values for 2 m above ground, a correction factor of 0.7479 was applied, based on a logarithmic wind speed profile (Allen et al., 1998).

Average annual precipitation in Salamat and Waza Logone are 807 mm and 709 mm, respectively. The rainy season is typically from May to September with maximum precipitation in July and August. Average annual values of ET_0 are 1718 mm in Salamat and 2011 mm in Waza Logone, exceeding annual precipitation by more than a factor of 2. However, in the second half of the rainy season, the monthly water balance is positive. The average water balance for July until September between 2003 and 2016 was 131 ± 101 mm $month^{-1}$ and 90 ± 63 mm $month^{-1}$ for Salamat and Waza Logone, respectively (Figure 2).

Chloride concentration was analyzed in the BGR laboratory in Hanover, Germany using a Thermo Fischer (Dionex) type ICS-5000 ion chromatograph with a detection limit of 0.003 mg l^{-1}. Concentration in ponding water was measured in four samples in Salamat, which varied between 2.5 mg l^{-1} and 25 mg l^{-1}.

Precipitation was sampled using a Hellmann rainwater collector in N'Djamena. This device was designed to minimize to a minimum evaporation by using a narrow soft polypropylene plastic tube of 4 mm inner diameter to connect the funnel on top of the device with the bottom of the 3 l collection bottle (Gröning et al., 2012). Once precipitation starts, water rises in the bottle and into the tube decoupling the atmosphere from the bottle headspace to prevent evaporation. To ensure that evaporation is as low as possible, sampling took place event-wise. Chloride concentration in precipitation was measured in 59 out of 147 samples collected in N'Djamena between 2014 and 2020 for different precipitation events and stages of the rainy season (Table S1). Not all rain samples could be analyzed for chloride concentration, due to limited sample volume in minor events at the beginning and end of the rainy season.

Average chloride concentration in May was 2.5 ± 2.3 mg l^{-1} (3 samples). Precipitation in June to September has relatively low chloride concentrations, declining from 0.6 ± 0.3 mg l^{-1} to 0.26 ± 0.12 mg l^{-1} and 0.38 ± 0.14 mg l^{-1} at the end of the season. Strong rain events in July and August have chloride concentrations between 0.2 and 0.3 mg l^{-1}. The annual wet chloride deposition sums to 1.8 ± 0.5 kg ha^{-1}. The measured values are in the range of published data (Goni et al., 2001; Laouali et al., 2012; Bouchez et al. 2019; Gebru and Tesfahunegn, 2019). Dry deposition of chloride is estimated between 10 – 30% of wet deposition (Bouchez et al. 2019).

2.3 Soil and vegetation data

At each study site, vertical soil profiles were core-drilled using a hand auger. In Salamat, soil profiles were sampled in 2016 (Tewolde et al., 2019) and 2019. In Waza Logone, soil samples were sampled in 2017 only (Tewolde et al., 2019), due to security reasons in 2019. Each of the soil profiles was sampled in 10 cm intervals and filled into headspace glass vials and plastic bags.

Each soil fraction was tested for grain size distribution using standard sieving and sedimentation procedures (Tewolde, 2017). Classification follows the soil texture triangle by the US Department of Agriculture (Šimůnek et al., 2011).

Chloride concentration was analyzed after aqueous extraction from oven dried (105°C for 24 hours) soil samples following the standard guideline DIN EN 12457-1 (Tewolde, 2017). Chloride concentrations in groundwater, which are used for comparison, were measured using a DIONEX ICS-3000 ion chromatograph. Data are presented in Tables S2 and S3

Gravimetric water content is the mass of water contained in a sample as a percentage of the dried soil mass. It was obtained by weighing the moist sample, oven drying it at 105°C for 24 to 48 hours, and weighing it again (Tables S2 and S3). Bulk densities were not measured in the field, because of the difficulties handling the samples end sending them to the laboratory. Instead, volumetric water contents were obtained by multiplying the gravimetric water contents for each soil type and location by typical bulk densities obtained from the Global Gridded Surfaces of Selected Soil Characteristics database (Global Soil Data Task Group, 2000), although accuracy of the calculated values reduces with sampling depth (Al-Shammary et al., 2018).

The type of vegetation and the annual cycle of crops, length of the flooding period, and vegetation throughout the dry period were mapped during field work and documented by surveying resident populations. In addition, MODIS vegetation indices data (Didan, 2015) were used to justify the documented annual cycle of phenology (Figure 3).

3 Modelling methodology

Our approach assumes that groundwater recharge is controlled by precipitation, evaporation, and transpiration (surface runoff can be neglected due to the flat topography). Soil moisture and chloride concentration along the soil profile at a certain time are indicators for evaporation and transpiration processes within the root zone. Chloride concentration in soil depends on its input via precipitation and washing out of dry deposition as well as on the amount of evaporation and transpiration on the soil surface and in the root zone. We assume that amount of recharge corresponds to the volume of water that leaves the model profile through the bottom boundary.

The first estimation of evapotranspiration was carried out using the FAO-dual crop coefficient approach that assesses E and T individually. The uncertainty of E and T partitioning on soil water and chloride concentration in the six soil profiles was assessed by considering scenarios of mean, maximum, and minimum E and T coefficients (see 3.1). Calculated time series of E and T for the site-specific vegetation were used to estimate soil water and chloride concentration profiles at the sampling time in each of the six locations using Hydrus-1D. A Bayesian approach was applied to consider uncertainties in chloride concentrations of precipitation and dry deposition, in partitioning E and T as well as in the parametrisation of the soil hydraulic model (Figure 4).

3.1 Partitioning of evaporation and transpiration

Evapotranspiration (ET) is the combination of two main processes driven by atmospheric demand: evaporation from the soil (E) and transpiration through the stomata of plants (T) and is an important component of the water balance, especially in semi-arid areas. The FAO provides a model (Allen et al., 1998) for estimating crop evaporation (ET_c) based on an empirically defined crop coefficient (K_c) combined with a reference evapotranspiration (ET_0). Two approaches are possible, single crop coefficient and dual crop coefficient. The latter was applied in this work.

The dual K_c method (Allen et al., 1998) is the sum of two coefficients, the basal crop coefficient (K_{cb}) that describes plant transpiration and the soil water evaporation coefficient (K_e) that depicts evaporation from the soil surface. K_{cb} is defined as the ratio of crop evapotranspiration over reference evapotranspiration (ET_c/ET_0), when the soil surface is dry and transpiration occurs at a potential rate (i.e. unlimited water availability for transpiration). K_e is highest when the topsoil is wet, but diminishes with drying out of topsoil to become zero, if no water remains near the soil surface for evaporation.

The parameters required for the estimation of monthly ET_c are the monthly reference evapotranspiration (ET_0), the monthly basal crop coefficient (K_{cb}) and the monthly soil water evaporation coefficient (K_e):

$$ET_c = ET_0 * K_c = ET_0 * (K_{cb} + K_e)\,, \quad (2)$$

Onsite information on vegetation and phenology, such as month of planting, full emergence of crops, and harvesting times, was used to define the monthly variation of vegetation at the study sites. These different vegetation periods were combined with crop-specific K_{cb} values for sorghum and grass provided in Allen et al. (1998) for a sub-humid climate with relative humidity of 45% and an average moderate wind speed of 2 m s^{-1}. To comply with the local semi-arid climate conditions in

Salamat and Waza Lagone, the coefficients K_{cb} for mid- and late-time vegetation periods were adjusted as proposed by Allen et al. (1998). Monthly K_{cb} values for Acacia were estimated based on Do and Rocheteau (2003) and Do et al. (2008). Site-specific monthly variation of ground cover and flooding periods with ranges of crop coefficient (K_{cb}), soil water evaporation coefficient (K_e), and root depth are provided in Table S4.

3.2 Modelling water flow and solute transport

3.2.1 Model concept, setup, and initial conditions

The chloride profiles measured in soil at a certain time represent water and solute budget input from past precipitation events and can be estimated by transient water flow and solute transport modelling. The model concept assumes that atmospheric chloride input is restricted to solute in precipitation and that the chloride concentration profile results from solute enrichment in the soil, due to evaporation and transpiration. An accurate parametrization of the unsaturated flow and transport model as well as a robust quantification of groundwater recharge are not possible with the available data and hence cannot be included within the scope of this study. However, the model results estimate groundwater recharge magnitude and variability based on information regarding soil texture and vegetation as well as associated uncertainty in results. This proposed approach is appropriate for locations with limited availability of long-term soil water measurements.

The free software package Hydrus-1D version 4.17.0140 was used to simulate transient water flow and solute transport in the six variably saturated soil profiles. Hydrus-1D numerically solves the Richards (1931) equation for variably saturated water flow, advection-dispersion equations for heat, and solute transport (Šimůnek et. al, 2009):

$$\frac{\partial \theta(h)}{\partial t} = \frac{\partial}{\partial z}\left[K(h)\left(\frac{\partial h}{\partial z} + cos\ \alpha\right)\right] - S(h) \quad (3)$$

with:

h	soil water pressure head [L]
θ	volumetric water content [L^3L^{-3}]
t	time [T]
z	spatial coordinate [L] (positive upwards)
S	sink term [$L^3L^{-3}L^{-1}$]
α	angle between flow direction and vertical axis
K(h)	unsaturated hydraulic conductivity function [LT^{-1}]

The processes simulated at the six study sites were water flow, solute transport, and root water uptake. Hydrus-1D requires input data at daily time steps, but available precipitation and evaporation data were monthly. Daily values were calculated dividing monthly data by month-specific days. Thus, all days in a month had the same precipitation rate and the same evapotranspiration rate. Model execution ended at the soil sampling time (December 2016 and July 2019 for Salamat and June 2017 for Waza Logone). Progressive root growth was considered in all profiles except for ST2, in which the roots of the Acacia

trees were distributed along the whole profile and assumed invariant over the simulation period. Since initial conditions of soil moisture and resident chloride concentration are unknown, arbitrary values were adopted. To account for different residence times of water and chloride, due to different degrees of evapotranspiration and unknown initial conditions, each model was run over a period of time long enough to allow the exchange of at least one water column volume. Thus, total modelling periods are different depending on the soil type at each site: ST1, ST2 start in 1910, which leads to a maximum residence time (MRT) of 106 years; ST3 in 2010 (MRT = 6 years), WL1 and WL2 in 1990 (MRT = 26 years), and WL3 in 1970 (MRT = 46 years). All profiles were discretized into 101 nodes and different horizons according to the soil types interpreted from the individual grain size distributions.

3.2.2 Water flow

For calculation of water retention (θ) and unsaturated hydraulic conductivity functions ($K(h)$), the Mualem-van Genuchten (MVG) model (van Genuchten, 1980) was applied:

$$\theta(h) = \begin{cases} \theta_r + \frac{\theta_s - \theta_r}{[1+|\alpha h|^n]^m} & h < 0 \\ \theta_s & h \geq 0 \end{cases} \quad (4)$$

$$k(h) = k_s S_e^{-1} \left[1 - \left(1 - S_e^{l/m}\right)^m\right] \quad (5)$$

where:

$$m = 1 - \frac{1}{n}; \qquad n > 1$$

$$S_e = \frac{\theta(h) - \theta_r}{\theta_s - \theta_r}$$

with

θ	water content [$L^3\ L^{-3}$]
h	hydraulic head [L]
θ_r	residual water content
θ_s	saturated water content
α	inverse of the air-entry value, empirical [L^{-1}]
n	pore-size distribution index, empirical [-]
l	pore-connectivity parameter, empirical ≈ 0.5 [-]
S_e	effective saturation [-]
k_s	saturated hydraulic conductivity [LT^{-1}]

To reduce computational effort, the initial parametrization of these functions was realized using pedotransfer functions implemented in Rosetta (Schaap et al., 2001), which is a dynamically-linked library coupled to Hydrus-1D. The input parameters for each profile were the percentages of sand, silt, clay, and bulk density at several depths. Whenever consecutive layers of a profile showed almost the same grain size distribution (texture) and soil moisture, the layers were lumped together and parameter averages were used in the model. The tortuosity parameter l [-] of the MVG was set to 0.5 as proposed by Mualem (1976).

The upper boundary condition was defined as a variable atmospheric condition, whereas the lower boundary was set to zero-gradient with free drainage of water for all profiles, except WL3 where confined groundwater conditions prevailed below the confining clay layer encountered at 3.9 m depth. During drilling, groundwater was hit at 3.9 m depth, but rapidly rose to 2.6 m below surface. Consequently, a constant head condition was implemented at 2.6 m depth.

3.2.3 Root water uptake and root growth

The sink term (S) in the Richards' equation, defined by Feddes et al. (1978) as the volume of water removed from a unit volume of soil per unit time due to plant water uptake, was considered in all soil profiles according to the prevailing vegetation (Table S4). The Feddes' default parameters for grass were used in the ST3 and Waza Logone profiles. In ST1, where sorghum was planted, Feddes' parameters for corn were used because sorghum is not available in the list. According to Righes (1980) sorghum and corn roots extract water from approximately the same soil depths and have similar average root density distribution.

An average root depth of 1 m was adopted in ST1 for the initial and end seasons, and 2 m for development and mid seasons. In the case of Acacia in ST2, the adopted parameters correspond to deciduous trees. The root depth of the Acacia tree was considered as constant over the entire simulation period with maximum root distribution at 0.5 m and decreasing distribution down to 2 m (Beyer et al., 2016). In ST3, the vegetation was defined as grass, while in WL1, WL2 and WL3 it was defined as grass with a flooding period of 3 months in WL1 and WL3, but only one month in WL2. Rooting depth values used at these sites range from 0.1 m to 0.5 m, depending on the growth stage of grass. The median maximum rooting depth value of annual grass in water-limited ecosystems is 0.37 m with a 95% confidence level in an interval of 0.26 m-0.55 m (Schenk and Jackson, 2002).

3.2.4 Solute transport

The chloride concentration in soil water was simulated using an equilibrium advection-dispersion model implemented in Hydrus1D. Hydrodynamic dispersion was implemented considering dispersivity values of 1/10th of the individual layer thickness, a molecular diffusion coefficient of 1.3×10^{-9} m^2s^{-1}, and a tortuosity factor as defined by Millington and Quirk (1961). Adopted dispersivity values are within reported ranges of 0.08 m to 0.20 m (Vanderborght and Vereecken, 2007; Stumpp et al, 2009, 2012).

A time-dependent concentration boundary condition was applied to the upper boundary and a zero-gradient boundary condition to the lower boundary. The transient liquid phase concentration of infiltrating rainwater follows measured chloride concentration in precipitation sampled in N'Djamena. The chloride concentration of ponding water correspond to four values measured in Salamat that range from 2.5 mg l^{-1} to 25 mg l^{-1} with an average of 9 mg l^{-1}. Initial chloride concentration in soil water was set to 0 mg l^{-1}. However, each model was run over a period of time long enough to allow the exchange of at least one water column volume (3.2.1). The model does not consider root solute uptake.

3.2.5 Crop evapotranspiration scenario definition

Since crop evapotranspiration was not measured, values were simulated using K_{cb}, K_e, and root depth instead. Because these parameters are given in ranges (Table S4), seven scenarios with different combinations of K_{cb}, K_e, and root depth were developed to assess ranges of crop evaporation (Table 2). Scenario "Mean" corresponds to the average value of all parameters. Scenarios "Min" and Max" combine the minimum and maximum values, respectively. Scenario "Mix-1" combines minimum K_{cb} with average K_e and root depth, scenario "Mix-2" minimum K_e with average K_{cb} and root depth whereas scenario "Mix-3" combines minimum root depth with average K_e and K_{cb}.

3.2.6 Bayesian model calibration

Based on the crop evapotranspiration scenarios, the models were calibrated and model uncertainty was estimated using a Bayesian calibration. Bayesian analysis is a combination of the data likelihood and the prior distribution using the Bayes theorem (ter Braak and Vrugt, 2008). The sum of likelihood functions for soil moisture and chloride concentration was implemented to calculate the log-likelihood of a simulation given the observations and standard deviations at each calibration step. The posteriori parameter distribution was estimated using the Differential Evolution Markov Chain Monte-Carlo (DE-MCzs) algorithm with three sub-chains (ter Braak and Vrugt, 2008) implemented in the R package BayesianTools (Hartig et al., 2019). The number of iterations was defined individually according to a Gelman-Rubin reduction factor < 1.2.

In the calibration, scaling factors ranging from 0.75 to 1.25 for the MVG parameters (saturated volumetric water content, alpha, and n) were adopted individually. However, ranges for the MVG model parameter n were constrained to n > 1.01. Log-transformed saturated hydraulic conductivity for each layer was considered with ranges from -0.5 to 0.5. The scaling factor for transpiration was simultaneously used as a divisor for evaporation to remain within the calculated rate of ET_0. From all accepted model runs, 100 were randomly selected at each individual location to evaluate average model results and standard deviations.

4 Results

4.1 Grain size distribution

Soil textures were defined based on grain size distributions of the six profiles (Figure 5) according to the US Department of Agriculture soil texture triangle. Most profiles are fine-grained soils (clay, sandy clay) and fine-grained soils with intercalation of thin sand and loam layers. Only soil profile ST3 is dominated by sand and sandy clay loam.

4.2 Model parametrization

The calibrated parametrization of the MVG model for each layer of the six sampling locations is plausible (Table 3). The posterior distributions of the Bayesian calibration show the sensitive parameters of the model fit. For ST1, these are n, θ_s, chloride concentration, and the transpiration fraction in evapotranspiration (T), but the k_s is less sensitive (Fig. S1). For ST2, the sensitivities of the model parameters are similar with k_s of the upper layer being the most sensitive and chloride concentration the least sensitive (Fig. S2). The model fits of the data from site ST3 are generally insensitive. Only α, n, and k_s of the upper layer as well as chloride concentration show tighter posteriori distributions (Fig. S3). For site WL1, the model parameters n of layers 1, 2, and 3 as well as the saturated water content of layers 3 and 5, and subordinately of layer 4, are sensitive (Fig. S4). For WL2, the model parameters n of all layers, k_s of layer 3, and θ_s of layers 2 and 3 are sensitive (Fig. S5). For WL3, θ_s of layer 2, k_s of layers 1 and 2, and the fraction of transpiration in evapotranspiration are sensitive (Fig. S6).

4.3 Soil water content, chloride concentration and groundwater recharge

Measured and simulated water content and chloride concentration profiles for individual scenarios are shown in Figure 6. The average root mean squared error (RMSE) of simulated water content for all individual scenarios ranges from 0.02 to 0.06 cm^3 cm^{-3} (Table 4). In general, the models reproduce well the water content and chloride concentrations. However, the dynamics of measured and simulated water contents differ considerably for ST1 and partly for ST2, although maximum values do match. This is due to the long chloride residence time in both locations (109 years) in comparison to the length of data availability (49 years for precipitation and 6 years for chloride concentrations). The models do not match the high chloride concentrations in the uppermost part of soil profiles for ST3, WL1, and WL2. The standard deviations in chloride concentration of the randomly selected model runs are exceptionally high in the lower part of ST2 that corresponds to the poor sensitivity of the chloride concentration at the upper boundary and the comparably wide range of measured chloride concentration in ponding water in the Salamat region (2.5 mg l^{-1} – 25 mg l^{-1}).

Measured chloride concentrations in groundwater are much lower compared to those in soil profiles (Tables S2 and S3). This is because groundwater encountered in the study area has been recharged in regions, where chloride input does not play an important role. Large amounts of recharge for the Quaternary aquifer occur mainly in the southern part of the Lake Chad Basin, where long-term annual precipitation reaches values over 1000 mm. Any chloride accumulated in the soil is well diluted and washed away periodically.

However, the large differences in chloride concentrations between soils and groundwater demonstrate the enormous accumulation capacity of soils in the Lake Chad Basin, which act as a buffer over years until precipitation is high enough to dilute the profile. This effect is depicted by the different chloride concentrations measured in profile ST1 between 2016 and 2019 (Table S2) and by the model results for profile ST2 (Figure 7).

The interannual variability of modelled groundwater recharge differs considerably among locations (Figure 7, Table 5). In general, interannual groundwater recharge variability depends on vegetation and soil texture with related water retention capacity. Vegetation with deep roots on soil with comparably high water retention capacity have a stronger interannual variability, e.g. at ST1, ST2 where recharge occurs only in years with high precipitation. Fine textured soils with shallow rooting vegetation have an intermediate variability (WL1, WL2, and WL3), where years without recharge occur only during drought periods. The coarser textured soils with grass cover have low interannual recharge variability (ST3) and recharge occurs each year. Years with high precipitation, e.g. 2006, 2007, and 2008 in Waza Logone as well as 2010 in Salamat, produced strong groundwater recharge.

The highest average annual recharge (93 mm) was calculated for ST3 in Salamat (Table 6), where the water balance during the rainy season (July-September) is higher compared to the Waza Logone region, and where shallow rooting vegetation prevails on comparably coarse soil texture with low water retention capacity and higher hydraulic conductivity. The other locations in Salamat have lower calculated annual recharge, due to deep rooting vegetation and higher soil water retention capacity. The impact of soil texture on annual groundwater recharge becomes apparent by comparing the three locations in Waza Logone with the same vegetation on soils with different water retention capacities and hydraulic conductivities. Groundwater recharge expressed as a fraction of precipitation is between 1% and 4% (Table 5), which is within the range of 0.1 to 5% published by Scanlon et al. (2006). Only at WL2 (8%) and ST3 (12%), where coarse soil textures enhance recharge, a comparably high fraction is estimated.

Simulated chloride concentration and water budget of the soils over the simulated time-period are rather unstable and differ for the six locations. At location ST2 with clay loam soil covered by Acacia and grass, accumulation of chloride takes place over several years, due to the high transpiration related to the effective field capacity. However, in high precipitation years, most of the accumulated chloride is leached to groundwater and soil concentration diminishes, which can be seen from the time-varying differences of the cumulative solute fluxes between the top and bottom boundaries (Figure 8). The difference of cumulative solute flux at the top and bottom boundaries represents the magnitude of chloride accumulation in soil. It should be noted that at this site, the measured chloride concentrations cannot be reconstructed, if only input via precipitation is considered. The measured profile can only be plausibly modelled with an additional input via ponding water. Chloride input at the upper boundary is consequently six-times higher at ST2 compared to the other locations considered in this study.

At location ST3, the chloride accumulation is much lower compared to the other locations. The chloride budget is controlled by the fast groundwater recharge response to precipitation, which flushes chloride annually from the soil towards the groundwater. Most of the chloride that infiltrated with precipitation remains in the vadose zone over several years and is

leached towards groundwater mainly during years with precipitation or water infiltration above threshold values (Figure 8). Chloride accumulation is highest in profiles with clay soils and high effective field capacity (ST1, WL1, and WL3).

Chemical memory effects are subject to the dynamics of the water and chloride balance. Therefore, steady-state assumptions are unsuitable. Accurate estimations are only possible with transient assumptions.

4.4 Evaporation and transpiration

The amount of transpiration depends on the availability of water in the root zone and the type of vegetation cover. At ST1, annual transpiration presents two peaks: one related to sorghum and the other to grass (Figure 9). At each location and in every simulation year, soil water content in the root zone reaches the wilting point defined by the specific parametrization of the root water uptake model.

The actual evaporation rate depends mainly on the availability of water in the upper soil zone (Table 6), but calculated values are in accordance with other studies in the area (Bouchez et al., 2019). Clay and clay-loam with relatively high water storativity have larger amounts of evaporated water compared to sand and loam soils. During dry seasons, the uppermost part of the soils dries up annually, which significantly restricts evaporation.

Actual evapotranspiration is lower than the reference evapotranspiration most of the year. During and shortly after the rainy season, when sufficient soil water is available, actual evapotranspiration is comparable to or higher than ET_0 depending on the vegetation.

5 Discussion

Soil texture information is helpful to constrain the MVG parameter ranges while searching for realistic parameter sets (Sprenger et al., 2015). However, poor representation of soil moisture dynamics using MVG parameters derived using Rosetta are reported (Sprenger et al., 2015) suggesting that soil structure has to be taken into account (Vereecken et al., 2010), especially for soils where high rock content influences water flow due to inherent heterogeneity (Sprenger et al., 2015). The soils at the locations considered in this study belong to Quaternary sediments in the Lake Chad basin and heterogeneity due to rock fragments is largely absent. Furthermore, soil moisture dynamics over the year are much higher in soils of the Waza Logone floodplain compared to soils from the more humid regions in the south, where annual precipitation, although high, occurs only over 4-5 months. It is expected that high soil moisture dynamics, rather homogeneous soils, and the monthly resolution of climate data result in a minor impact of soil structure on MVG parametrization and groundwater recharge as shown in Section 3.2. Soil moisture dynamics at all locations considered in this study are limited by water availability for evaporation in the uppermost part of the soil and by water uptake in the root zone, but not by the reference evapotranspiration. However, because time resolution of precipitation and evapotranspiration data is monthly, the models probably underestimate soil moisture dynamics.

Calculated chloride concentrations for the soil profiles give indications of appropriate MVG parametrization as well as evaporation and transpiration partitioning. However, uncertainty of chloride input and its transient variability in particular is

expressed in rather wide and partly bimodal distributions of the scaling factor (sc_Conc) included in the calibration (Figures S1-S6 in supplement material). On one hand, measured chloride concentrations in precipitation are in agreement with other studies in central Africa (Goni et al., 2001; Laouali et al., 2012; Gebru and Tesfahunegn, 2019) and its transient behaviour within the rainy season is considered in the applied model. On the other hand, impact of dry deposition is unknown, because of data scarcity and potential lateral flow of periodic flooding. Furthermore, due to the monthly resolution of the atmospheric boundary condition, extreme rain events that cause surface runoff cannot be reflected in the model. The variability of chloride concentration in some of the soil profiles, which cannot be completely reproduced by the model, indicates either a higher variability of chloride input and/or a larger variability in soil physics.

Bouchez et al. (2019) identified a chloride deficit between deposition and river export in the Chari-Logone river system of 88% (only 12% of the deposited chloride is exported via river water). They refer to the chemical memory effect, which can play an important role in arid regions. Our simulations show the importance of the vadose zone for storage of chloride over longer periods of time, which explains the fate of chloride in the basin and confirms the chemical memory effect. In this context, it must be noted that the thickness of the vadose zone at the locations considered in this study is between 4 m and 21 m, where important amounts of chloride can be potentially stored leading to a strong delay of the chemical signal from precipitation to groundwater.

Time-dependent recharge cannot be verified with groundwater hydrographs, because these data are not available in the study area. However, the calculated mean annual groundwater recharge values are within the ranges of 0.2 to 35 mm yr^{-1} estimated by Edmunds et al. (2002) using the CMB method in seven chloride profiles in northern Nigeria. The larger values (90 mm yr^{-1} in ST3 and 54 mm yr^{-1} in WL2) are due to local coarse soil and fall within the values estimated by Bouchez et al. (2019), who, based on ^{36}Cl and Cl budgets in groundwater, propose recharge values between 16 mm yr^{-1} and 240 mm yr^{-1}.

6 Conclusions

The quantitative estimation of groundwater recharge in the LCB is difficult due to the scarce data availability and the expected low recharge quantities. Estimation of low recharge amounts in arid and semi-arid areas are usually ambiguous, because the inherent measurement inaccuracies lead to uncertainties during data processing and modelling. Quantification of water and solute fluxes in the vadose zone is often implemented using long-term time series of soil moisture, pressure heads, and concentration data in combination with appropriate models. Monitoring of soil moisture and solute concentration over longer periods at different depths and sites is difficult in the LCB, due to limited infrastructure and challenging climatic boundary conditions. The presented approach combines soil moisture and chloride concentration quantified along vertical soil profiles in different locations within the LCB with numerical models and freely accessible data, while considering data uncertainty. Calculated chloride concentrations for the soil profiles provide appropriate MVG parametrization as well as evaporation and transpiration partitioning. Although measured and simulated dynamic behaviour of both water contents and chloride concentrations differ considerably in profiles ST1 and partly in ST2, their magnitudes largely agree. This is especially important for chloride concentrations in the middle and deeper parts of the profiles, where seasonal effects are mainly averaged.

Thus, the estimates of soil water balance and especially of groundwater recharge as well as the adopted soil physical parameters are plausible.

Mean groundwater recharge values estimated in this study are different from those published in Tewolde et al. (2019). This is due to the more extensive availability of chloride concentration data in precipitation for this study. In addition, Tewolde et al. (2019) roughly estimated one value of saturated porosity for each profile. This parameter is rather sensitive in the Bayesian calibration and several values along each of the profiles were considered in this study. In contrast to the assessment of groundwater recharge with the CMB (Tewolde et al., 2019), the method used here allows not only estimates of mean recharge, but also its interannual dynamics, variability, and the classification of the uncertainties of the input data and modelling results. The interannual variability of groundwater recharge is generally higher than the uncertainty of the modelled groundwater recharge. The soil moisture dynamics at all locations considered in this study are limited by water availability for evaporation in the uppermost part of the soil and by water uptake in the root zone and not by the reference evapotranspiration.

Simulations show the importance of the vadose zone for storage of chloride over longer time-periods and explain the fate of chloride in the basin. The thickness of the vadose zone at the locations considered in this study varies between 4 m and 21 m. Important amounts of chloride can be potentially stored significantly delaying the chemical signal from precipitation to groundwater.

Upscaling of the results to larger areas must be interpreted with caution since the considered combinations of soils and vegetation probably do not cover all combinations present in the Salamat and Waza Logone regions.

Code availability

The software HYDRUS 1D belonging to the U.S. Department of Agriculture was used. The latest version of the program can be downloaded from https://www.ars.usda.gov/research/software/download/?softwareid=97&modecode=20-36-15-00.

Author contribution

M.R. conducted fieldwork; A.G.M.S. and C.N. conducted modelling and interpretation; C.N. and S.V. designed the study and completed the writing. All authors contributed to the discussion of results and commented on the manuscript.

Competing interests

The authors declare that they have no conflict of interest.

Acknowledgement

This study was conducted within the framework of the technical cooperation project “Lake Chad Basin - Management of Groundwater Resources” jointly executed by the Lake Chad Basin Commission (LCBC) and the German Federal Institute for Geosciences and Natural Resources (BGR). The technical project is funded by the German Federal Ministry for Economic

Cooperation and Development (BMZ). We thank Daniel Tewolde, Paul Königer and Anna Degtjarev for their support in the lab. We are highly indebted to John Molson for the thorough linguistic review of our manuscript.

References

Allen, R. G., Pereira, L. S., Dirk, R., Smith, M.: Crop evapotranspiration: Guidelines for computing crop water requirements. FAO Irrigation and Drainage Paper No. 56. Rome, Italy. https://doi.org/10.1016/j.eja.2010.12.001, 1998.

Al-Shammary, A. A. G., Zouzani, A. Z., Kaynak, A., Khoo, A. Y. Norton, M. Gates, W.: Soil bulk estimation methods: A review. Pedosphere, 28(4), 581-596. https://doi.org/10.1016/S1002-0160(18)60034-7, 2018.

Alves, M. E. B., Mantovani, E. C., Sediyama, G. C., Neves, J. C. L.: Estimate of the crop coefficient for Eucalyptus cultivated under irrigation during initial growth. Cerne, 19(2), 247–253. https://doi.org/10.1590/s0104-77602013000200008, 2013

Anderson, R. G., Zhang, X., Skaggs, T. H.: Measurement and Partitioning of Evapotranspiration for Application to Vadose Zone Studies. Vadose Zone Journal, 16(13), 0. https://doi.org/10.2136/vzj2017.08.0155, 2017

Aouade, G., Ezzahar, J., Amenzou, N., Er-Raki, S., Benkaddour, A., Khabba, S., Jarlan, L.: Combining stable isotopes, Eddy Covariance system and meteorological measurements for partitioning evapotranspiration, of winter wheat, into soil evaporation and plant transpiration in a semi-arid region. Agricultural Water Management, 177, 181–192. https://doi.org/10.1016/J.AGWAT.2016.07.021, 2016.

Bader, J., Lemoalle, J., Leblanc, M.: Modèle hydrologique du Lac Tchad, Hydrolog. Sci. J., 56, 411–425, 2011.

Batello, C., Marzot, M., Harouna Touré, A.: The future is an ancient lake: Traditional knowledge, biodiversity and genetic resources for food and agriculture in the Lake Chad basin ecosystems. FAO Interdepartmental Working Group on Biological Diversity for Food and Agriculture, Rome, 2004.

Bernacsek, G. M., Hughes, J. S., Hughes, R. H. (Ed.): A directory of African wetlands. International Union for the Conservation of Nature and Natural Resources, 1992.

Beyer, M., Koeniger, P., Himmelsbach, T.: Constraining water uptake depths in semi-arid environments using stable water isotopes Results & Discussion. https://doi.org/10.5281/zenodo.56159, 2016.

Boronina, A., Favreau, G., Coudrain, A., Dieulin, C., Zairi, R.: Data scarcity in the large semiarid Lake Chad basin: incorporating environmental tracers as a priori information for groundwater modelling. ModelCare 2005, Scheveningen, The Netherlands, 2005.

Bouchez, C., Goncalves, J., Deschamps, P., Vallet-Coulomb, C., Hamelin, B., Doumnang, J.C., Sylvestre, F.: Hydrological, chemical, and isotopic budgets of Lake Chad: a quantitative assessment of evaporation, transpiration and infiltration fluxes, Hydrol. Earth Syst. Sci., 20, 1599–1619, 2016.

Bouchez, C., Deschamps, P., Goncalves, J., Hamelin, B., Nour, A.M., Vallet-Coulomb, C., Sylvestre, F: Water transit time and active recharge in the Sahel inferred by bomb-produced 36Cl. Nature, scientific reports, 9: 7465, 2019.

Carmouze, J.-P.: Originalité de la régulation saline du lac Tchad, Comptes Rendus de l'Académie des Sciences. Série D: Sciences Naturelles, 275, 1871–1874, 1972.

Cuthbert, M. O., Taylor, R.G., Favreau, G. et al.: Observed controls on resilience of groundwater to climate variability in sub-Saharan Africa. Nature, 572: 230-234. https://doi.org/10.1038/s41586-019-1441-7, 2019.

Didan, K.: MOD13Q1 MODIS/Terra Vegetation Indices 16-Day L3 Global 250m SIN Grid V006. NASA EOSDIS Land Processes DAAC. https://doi.org/10.5067/MODIS/MOD13Q1.006, 2015.

Didane, D. H., Rosly, N., Zulkafli, M. F., Shamsudin, S. S.: Evaluation of wind energy potential as a power generation source in Chad. International Journal of Rotating Machinery, vol. 2017, Article ID 3121875, 10 pp, 2017.

Do, F., Rocheteau, A.: Cycle annuel de transpiration d'Acacia raddiana par la mesure des flux de sève brute (Nord-Sénégal). In Un arbre au désert: Acacia raddiana (pp. 119–142). Paris, 2003.

Do, F., Rocheteau, A., Diagne, A. L., Goudiaby, V., Granier, A., Lhomme, J. P.: Stable annual pattern of water use by Acacia tortilis in Sahelian Africa. Tree Physiology, 28(1), 95–104. https://doi.org/10.1093/treephys/28.1.95, 2008.

Eberschweiler, Ch.: Suivi et gestion des ressources en eaux souterraines dans le bassin du lac Tchad – Prémodélisation des systèmes aquifères, évaluation des ressources et simulation d'exploitation. Rapport. BRGM/CBLT.

Edmunds, W. M., Gaye, C.B.: Estimating the spatial variability of groundwater recharge in the Sahel using chloride. J. Hydrol., 156(1-4):47-59, 1994.

Edmunds, W. M., Fellman, E., Goni, I. B.: Spatial and temporal distribution of groundwater recharge in northern Nigeria. Hydrogeology Journal, 10:205-215, 2002.

Feddes, R. A., Kowalik, P. J., Zaradny, H.: Simulation of field water use and crop yield. Published in 1978 in Wageningen by Centre for agricultural publishing and documentation. Wageningen: Centre for Agricultural Pub. and Documentation. https://lib.ugent.be/catalog/rug01:000032129, 1978.

Fontes, J.-C., Maglione, G., Roche, M.-A.: Données isotopiques préliminaires sur les rapports du lac Tchad avec les nappes de la bordure nord-est, Cah. Orstom. Hydrobiol., 6, 17– 34, 1969.

Fontes, J.-C., Gonfiantini, R., Roche, M.-A. : Deuterium et oxygène-18 dans les eaux du Lac Tchad. Isotope Hydrology, IAEA-SM-129/23, 1970.

Gebru, T.A., Tesfahunegn, G.B.: Chloride mass balance for estimation of groundwater recharge in a semi-arid catchment of northern Ethiopia. Hydrogeology Journal, 27:363-378, 2019.

Global Soil Data Task Group: Global Gridded Surfaces of Selected Soil Characteristics (IGBP-DIS). ORNL DAAC, Oak Ridge, Tennessee, USA. https://doi.org/10.3334/ORNLDAAC/569, 2000.

Goni, I., Fellman, E., Edmunds, W.: Rainfall geochemistry in the Sahel region of northern Nigeria, Atmos. Environ., 35, 4331–4339, 2001.

Goni, I., Taylor, R., Favreau, G., Shamsudduha, M., Nazoumou, Y., Ngouno Ngatcha, B.: Groundwater recharge from heavy rainfall in the southwestern Lake Chad Basin: evidence from isotopic observations. Hydrological Sciences Journal. https://doi.org/10.1080/02626667.2021.1937630, 2021.

Groh, J., Stumpp, C., Lücke, A., Pütz, T., Vanderborght, J., Vereecken, H.: Inverse estimation of soil hydraulic and transport parameters of layered soils from water stable isotopes and lysimeter data, Vadose Zone Journal 17:170168. https://doi.org/10.2136/vzj2017.09.0168, 2018.

Gröning, M., Lutz, H.O., Roller-Lutz, Z., Kralik, M., Gourcy, L., Pöltenstein, L.: A simple rain collector preventing water re-evaporation dedicated for $\delta^{18}O$ and $\delta^{2}H$ analysis of cumulative precipitation samples. J. Hydrol. 448-449, 195-200, 2012.

Harris, I., Osborn, T. J., Jones, P., Lister, D.: Version 4 of the CRU TS monthly high-resolution gridded multivariate climate dataset. Sci. Data 7, 109. https://doi.org/10.1038/s41597-020-0453-3, 2020.

Isihoro, S., Matisoff, G., Wehn, K.: Seepage relationship between Lake Chad and the Chad Aquifers, Groundwater, 34, 819–826, 1996.

Hartig, F., Minunno, F., Paul, S.: BayesianTools: General-Purpose MCMC and SMC Samplers and Tools for Bayesian Statistics, 2019.

Jasechko, S., Sharp, Z. D., Gibson, J. J., Birks, S. J., Yi, Y., Fawcett, P. J.: Terrestrial water fluxes dominated by transpiration, Nature, 496, 347–350, 2013.

Kool, D., Agam, N., Lazarovitch, N., Heitman, J. L., Sauer, T. J., Ben-Gal, A.: A review of approaches for evapotranspiration partitioning. Agricultural and Forest Meteorology, 184, 56–70, 2014.

Lake Chad Basin Commission: Monitoring and management of groundwater resources in the Lake Chad Basin. Mapping of aquifers, water resources management, final report, R35985, Report BRGM R 35985 EA U/4S/93, 1993.

Lake Chad Basin Commission: Report on the State of the Lake Chad Basin Ecosystem. http://www.cblt.org/sites/default/files/download_documents/report_on_the_state_of_the_lake_chad_basin_ecosystem.pdf, 2012.

Laouali, D., Galy-Lacaux, C., Diop, B., Delon, C., Orange, D., Lacaux, J.P., Akpo, A., Lavenu, F., Gardrat, E., Castera, P.: Long term monitoring of the chemical composition of precipitation and wet deposition fluxes over three Sahelian savannas. Atmos. Environ. 50, 314–327. https://doi.org/10.1016/j.atmosenv.2011.12.004, 2012.

Leblanc, M.: Gestion des ressources en eau des grands bassins semi-arides à l'aide de la télédétection et des SIG: application à l'étude du bassin du lac Tchad, Afrique, PhD thesis, Université de Poitiers, Poitiers, 2002.

Leblanc, M.: The Use of Remote Sensing and GIS for Water Resources Management of Large Semi-Arid Regions : a Case Study of the Lake Chad Basin, Africa. PhD Thesis, University of Glamorgan and University of Poitiers, 2002.

Leblanc, M., Favreau, G., Tweed, S., Leduc, C., Razack, M., Mofor, l.: Remote sensing for groundwater modelling in large semiarid areas: Lake Chad basin, Africa. Hydrogeology Journal, 15(1), 97-100, 2007.

Lemoalle, J., Bader, J.-C., Leblanc, M., Sedick, A.: Recent changes in Lake Chad: observations, simulations and management options (1973–2011), Global Planet. Change, 80, 247–254, 2012.

Lemoalle, J., Magrin, G.: Le développement du lac Tchad: situation actuelle et futurs possibles. Marseille, IRD Éditions, coll. Expertise collégiale, bilingue français-anglais, 216 p., 2014.

Lloyd, J. W.: A review of aridity and groundwater, Hydrological Processes, Vol. 1, 63-78, 1986.

Lloyd, J. W.: Groundwater in arid and semiarid regions. In: Silveira, L. and Usunoff E.J. [Eds.]: Groundwater (Vol. I), Encyclopedia of Life Support Systems, pp. 284–307, 2009.

Majnooni-Heris, A., Sadraddini, A. A., Nazemi, A. H., Shakiba, M. R., Neyshaburi, M. R., Tuzel, I. H.: Determination of single and dual crop coefficients and ratio of transpiration to evapotranspiration for canola. Annals of Biological Research, 3(4), 1885–1894, 2012.

Massuel, S.: Modélisation hydrodynamique de la nappe phréatique quaternaire du bassin du lac Tchad. Diplôme d'études approfondies, Université de Montpellier II, Université d'Avignon et des pays du Vaucluse, 2001.

Mertens, J., Barkle, G. F., Stenger, R.: Numerical analysis to investigate the effects of the design and installation of equilibrium tension plate lysimeters on leachate volume, Vadose Zone Journal, 4:488-499, 2005.

Millington, R. J., Quirk, J. P.: Permeability of porous solids. Trans. Int. Congr. Soil Sci., 7(1), 97-106, 1961.

Mualem, Y.: A new model for predicting the hydraulic conductivity of unsaturated porous media, Water Resour. Res., 12, 513–522. https://doi.org/10.1029/WR012i003p00513, 1976.

Ngatcha, B. N., Mudry, J., Leduc, C.: The state of understanding on groundwater recharge for the sustainable management of transboundary aquifer in the Lake Chad basin, 2008.

Olivry, J., Chouret, A., Vuillaume, G., Lemoalle, J., Bricquet, J.: Hydrologie du lac Tchad, Editions de l'ORSTOM, Paris 1996.

Richards, L. A.: Capillary conduction of liquids through porous mediums. Physics, 1(5), 318-333, 1931.

Righes, A. A.: Water uptake and root distribution of soybeans, grain sorghum and corn. Retrospective Theses and Dissertations. Iowa State University, 1980.

Roche, M.: Tracage naturel salin et isotopique des eaux du systeme du Lac Tchad, These de Doctorat d'Etat, Travaux et Documents de l'ORSTOM, ORSTOM (Office de la Recherche Scientifique et Technique d'Outre-Mer) editions, Paris, 1980.

Scanlon, B. R., Keese, K. E., Flint, A. L., Flint, L. E., Gaye, C. B., Edmunds, W. M., Simmers. I.: Global synthesis of groundwater recharge in semiarid and arid regions. Hydrol. Process. 20, 3335-3370, 2006.

Schaap, M. G., Leij, F. J., van Genuchten, M. T.: ROSETTA: a computer program for estimating soil hydraulic parameters with hierarchical pedotransfer functions, Journal of Hydrology, 251, 163-176, 2001.

Schenk, H. J., Jackson, R. B.: Rooting depths, lateral root spreads and belowground aboveground allometries of plants in water limited ecosystems. Journal of Ecology, 90, 480–494. https://doi.org/10.1046/j.1365-2745.2002.00682.x, 2002.

Shahrokhnia, M. H., Sepaskhah, A. R.: Single and dual crop coefficients and crop evapotranspiration for wheat and maize in a semi-arid region. Theoretical and Applied Climatology, 114(3–4), 495–510. https://doi.org/10.1007/s00704-013-0848-6, 2013.

Šimůnek, J., Sejna, M., Saito, H., Sakai, M., van Genuchten, M. T.: The HYDRUS-1D software package for simulating the one-dimensional movement of water, heat, and multiple solutes in variably-saturated media, Version 4.15, Riverside, California, 2009.

Šimůnek, J., Šejna, M., van Genuchten, M. T.: The HYDRUS Software Package for Simulating the Two- and Three-Dimensional Movement of Water, Heat, and Multiple Solutes in Variably-Saturated Media. Prague, 2011.

Sprenger, M., Volkmann, T. H. M., Blume, T., Weiler, M.: Estimating flow and transport parameters in the unsaturated zone with pore water stable isotopes, Hydrol. Earth Syst. Sci., 19(6), 2617-2635. https://doi.org/10.5197/hess-19-2617-2015, 2015.

Stumpp, C., Nützmann, G., Maciejewski, S., Maloszewski, P.: A comparative modeling study of a dual tracer experiment in a large lysimeter under atmospheric conditions, Journal of Hydrology, 375, 566-577, 2009.

Stumpp, C., Stichler, W., Kandolf, M., Šimůnek, J.: Effects of land cover and fertilization method on water flow and solute transport in five lysimeters: a long-term study using stable water isotopes, Vadose Zone Journal, 11(1). https://doi.org/10.2136/vzj2012.0075, 2012.

ter Braak, C.J.F., Vrugt, J.A.: Differential Evolution Markov Chain with snooker updater and fewer chains. Stat. Comput. 18, 435–446. https://doi.org/10.1007/s11222-008-9104-9, 2008.

Tewolde, D. O.: Investigating unsaturated zone water transport processes by means of biogeochemical analysis of soil depth profiles: a comparative study of two semi-arid sites. M.Sc.-Thesis, Leibniz Universitaet Hannover, 2017.

Tewolde, D. O., Koeniger, P., Beyer, M., Neukum, C., Gröschke, M., Ronnelngar, M., Rieckh, H., Vassolo, S.: Soil water balance in the Lake Chad Basin using stable water isotope and chloride of soil profiles. Isot. Environ. Health Stud. 55, 459-477. https://doi.org/10.1080/10256016.2019.1647194, 2019.

Tong, G. D., Liu, H. L., Li, F. H.: Evaluation of dual crop coefficient approach on evapotranspiration calculation of cherry trees. International Journal of Agricultural and Biological Engineering, 9(3), 29–39. https://doi.org/10.3965/j.ijabe.20160903.1886, 2016.

Vanderborght, J., Vereecken, H.: Review of dispersivity for transport modeling in soils, Vadose Zone Journal, 6(1), 29-52, https://doi.org/20.2136/vzj2006.0096, 2007.

van Genuchten, M. T.: A close-form equation for predicting the hydraulic conductivity of unsaturated soils 1, Soil Science Society of America Journal, 8(44), 892-898, 1980.

van Looy, K., Bouma, J., Herbst, M., Koestel, J., Minasny, B., Mishra, U., Montzka, C., Nemes, A., Pachepsky, Y. A., Padarian, J., Schaap, M. G.: Pedotransfer functions in earth system science: challenges and perspectives, Reviews of Geophysics, 55(4), 1199-1256. https://doi.org/10.1002/2017RG000581, 2017.

Vaquero, G., Siavashani, N.S., García-Martínez, D., Elorza, J., Bila, M., Candela, L., Serrat-Capdevila, A.: The Lake Chad transboundary aquifer. Estimation of groundwater fluxes through international borders from regional numerical modelling. Journal of Hydrology: Regional Studies, 38 p. https://doi.org/10.1016/j.ejrh.2021.100935, 2021.

Vassolo. S.: The aquifer recharge and storage systems to reduce the high level of evapotranspiration. In: Adaptive Water Management in the Lake Chad Basin. World Water Week 09, FAO, pp. 30-44, 2009.

Vereecken, H., Javaux, M., Weynants, M., Pachepsky, Y. A., Schaap, M. G., van Genuchten M. T.: Using pedotransfer functions to estimate the van Genuchten-Mualem soil hydraulic properties: A review, Vadose zone Journal, 9(4), 759-820. https://doi.org/10.2136/vzj2010.0045, 2010.

Vereecken, H., Schnepf, A., Hopmans, J. W., Javaux, M., Or, D., Roose, T., … Young, I. M.: Modeling soil processes: Review, key challenges, and new perspectives, Vadose Zone Journal, 15(5), 1-57. https://doi.org/10.2136/vzj.2015.09.0131, 2016.

Vieira, P. V. D., de Freitas, P. S. L., Ribeiro da Silva, A. L. B., Hashiguti, H. T., Rezende, R. Junior, C. A. F.: Determination of wheat crop coefficient (K_c) and soil water evaporation (K_e) in Maringa, PR, Brazil, African Journal of Agricultural, 11(44), 4551–4558. https://doi.org/10.5897/AJAR2016.11377, 2016.

Vuillaume, G.: Bilan hydrologique mensuel et modélisation sommaire du régime hydrologique du lac Tchad, Cahiers ORSTOM. Série Hydrologie, 18, 23–72, 1981.

Wu, Y., Du, T., Ding, R., Tong, L., Li, S.: Multiple Methods to Partition Evapotranspiration in a Maize Field. Journal of Hydrometeorology, 139–149. https://doi.org/10.1175/JHM-D-16-0138.1, 2016.

Zairi, R.: Étude géochimique et hydrodynamique du Bassin du Lac Tchad (la nappe phréatique dans les régions du Kadzell (Niger oriental) et du Bornou (Nord-Est du Nigéria)), PhD thesis, Université de Montpellier 2, Montpellier, 2008.

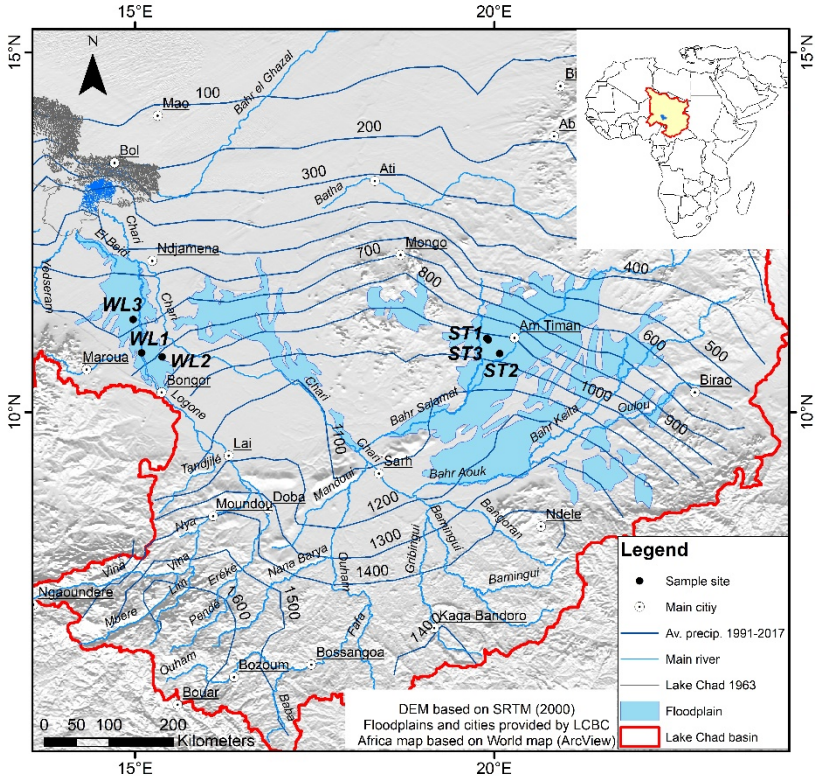

Figure 1: Location of the six soil sampling sites within the Logone and Salamat river basins in the Lake Chad catchment. The map inset shows the location of the Lake Chad basin in Africa.

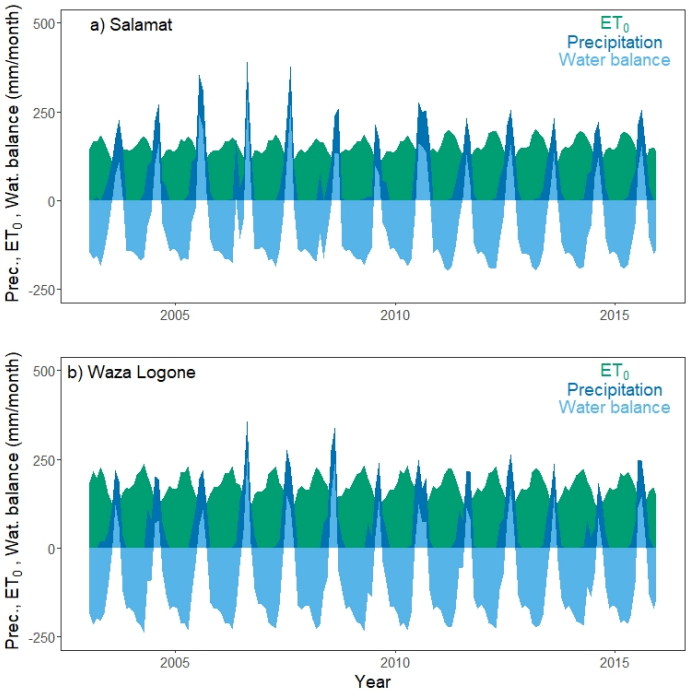

Figure 2: Monthly precipitation, reference evapotranspiration from the CRUTS 4 database (NCAR, 2017) and derived water balance for Salamat and Waza Logone.

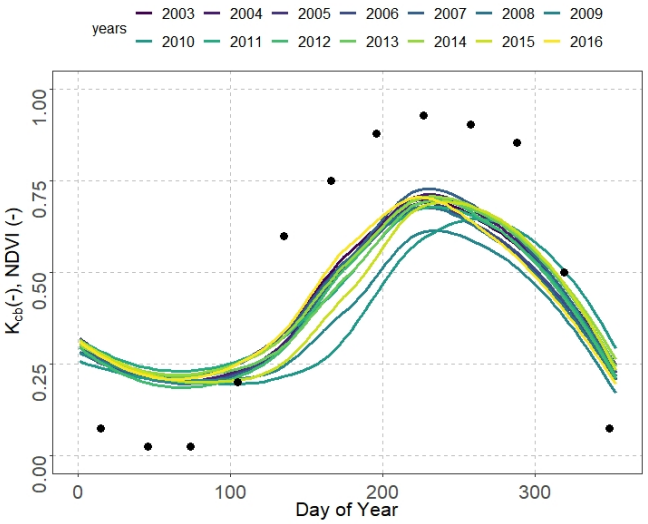

Figure 3: Average Normalized Difference Vegetation Index (NDVI, MODIS 16 day interval and 250 m spatial resolution) measured between 2003 and 2016 in the Salamat region and estimated monthly basal crop coefficient (K_{cb}, black points) for location S3.

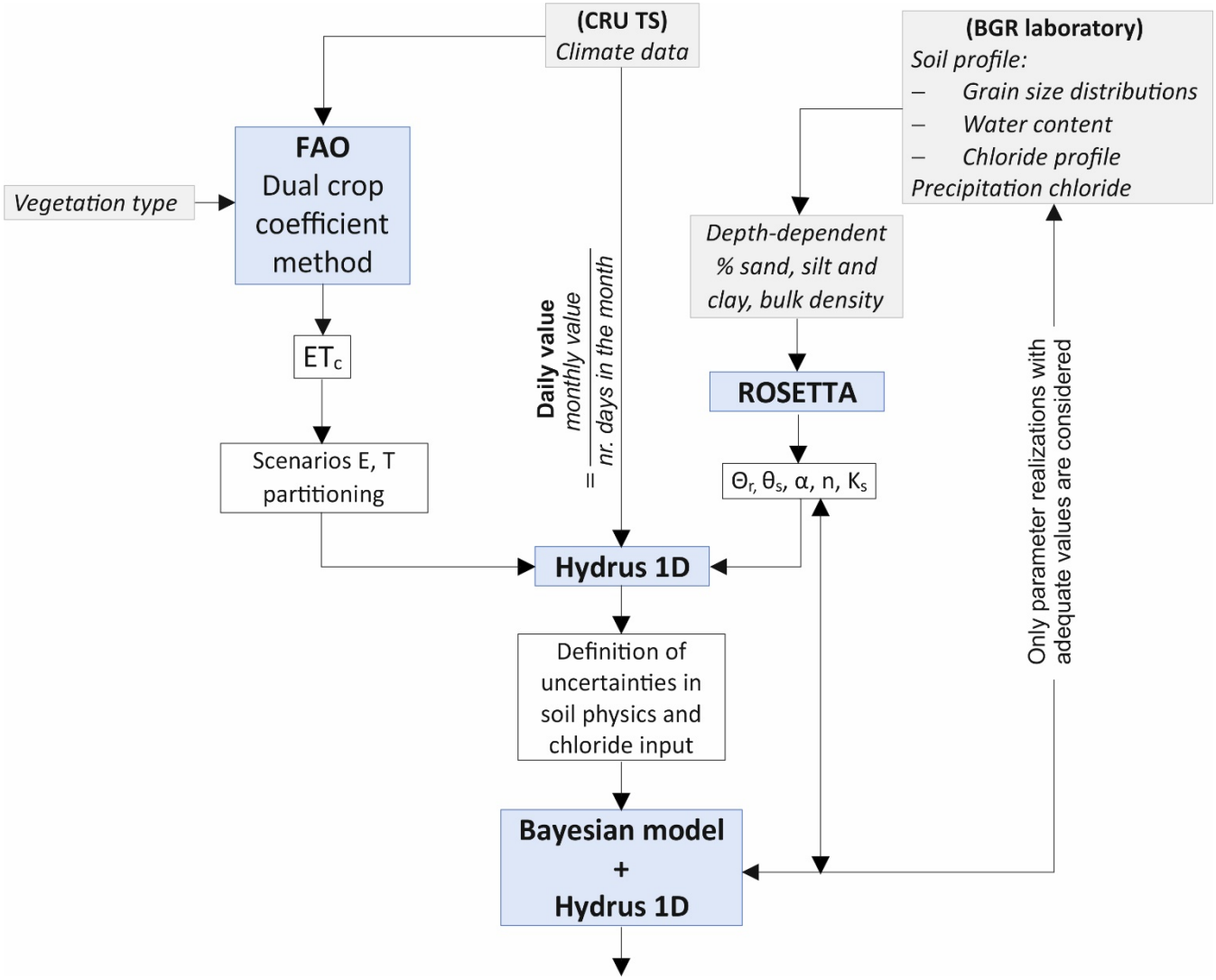

Figure 4: Workflow of the modelling activities

Figure 5: Soil textures used in the model (left column) defined according to the grain size distribution analysis (right column) for each of the six soil profiles.

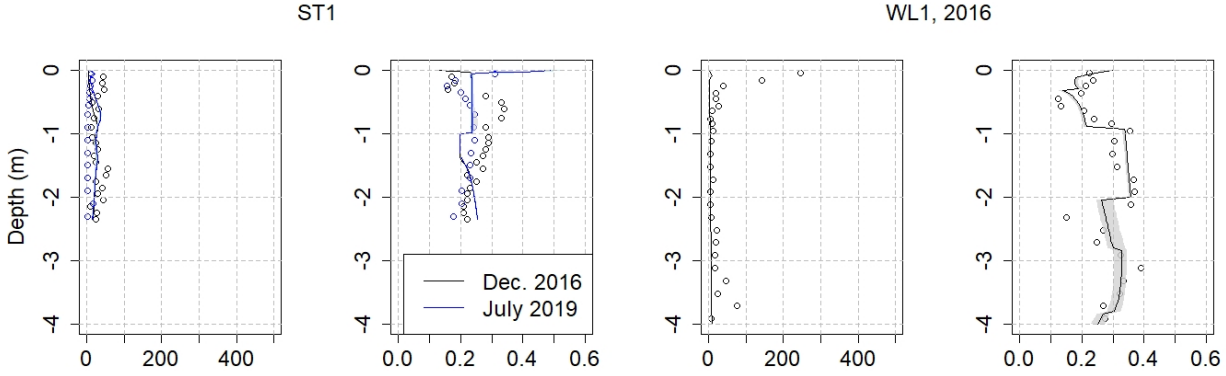

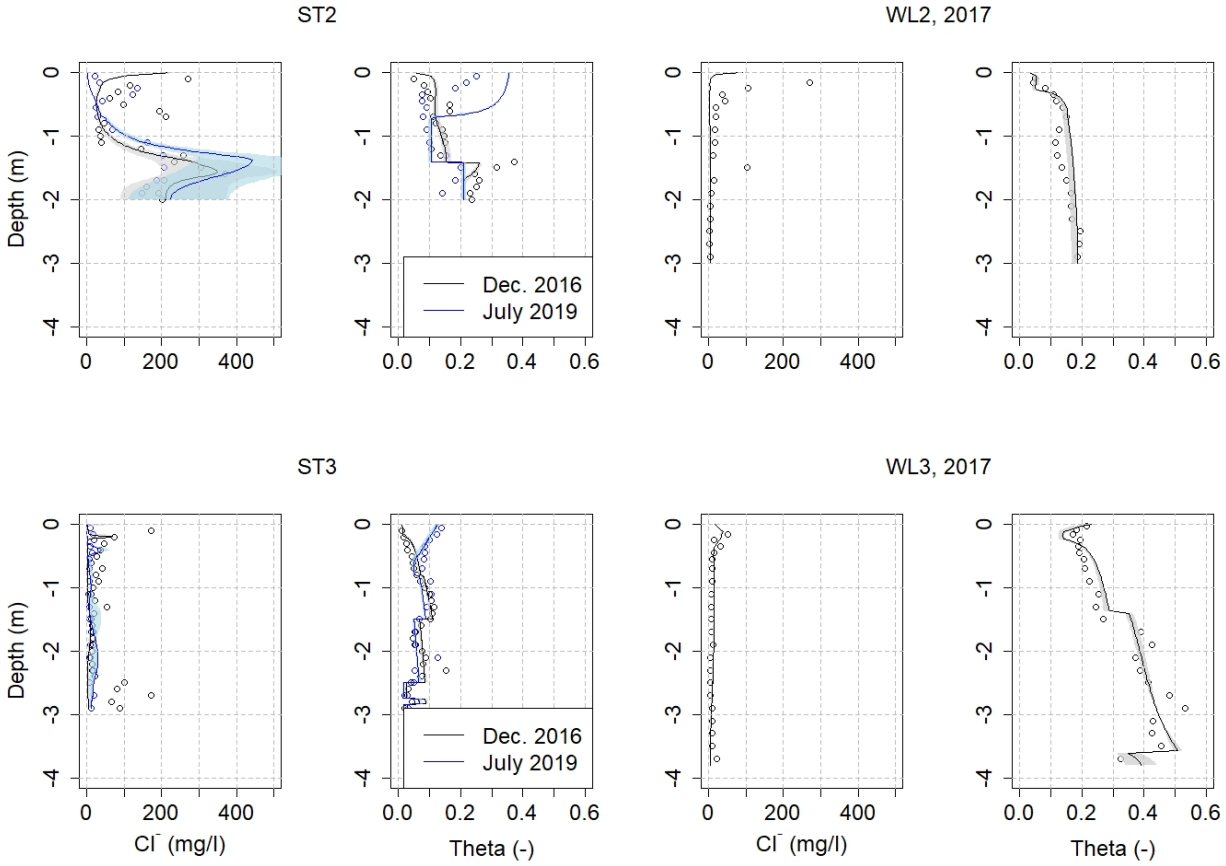

Figure 6: Measured and simulated scenarios of chloride concentration and water content for all six soil profiles. Shaded areas represent the standard deviation of 100 randomly selected model runs.

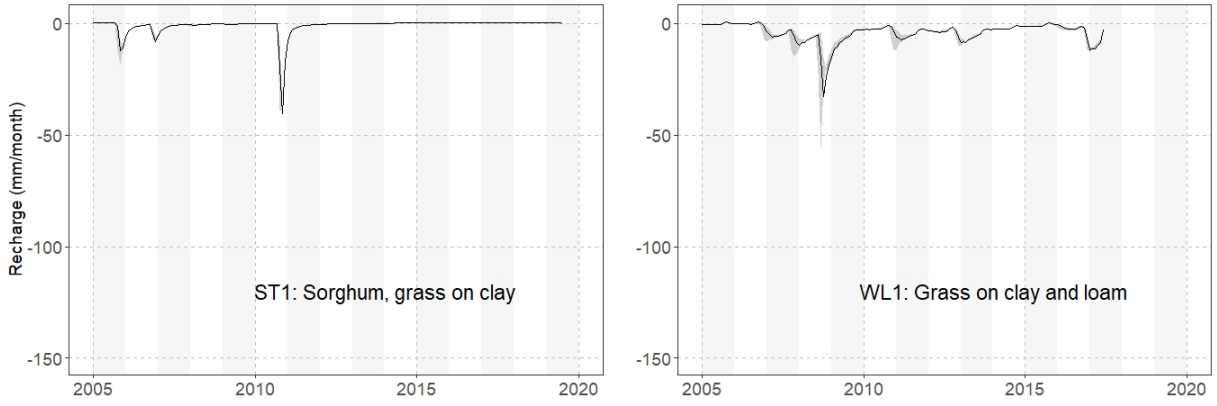

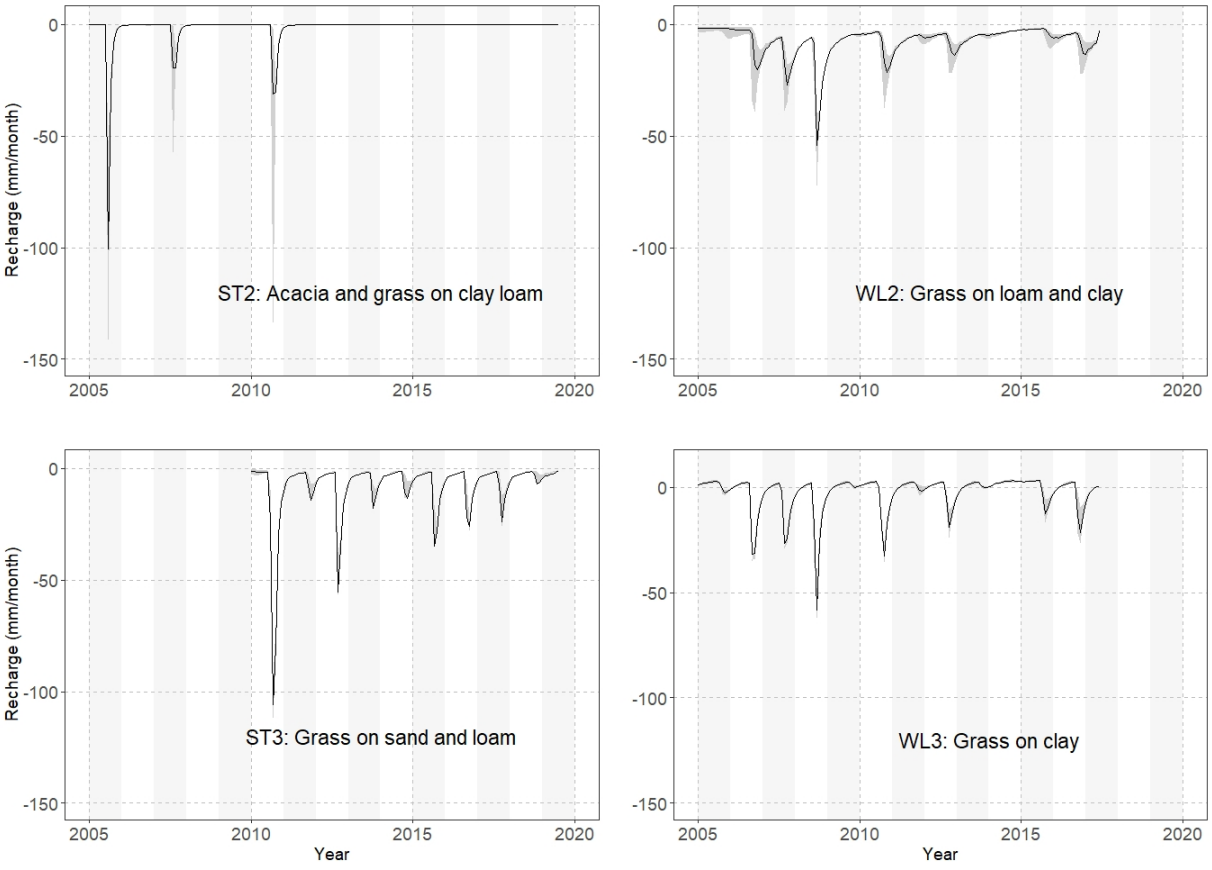

Figure 7: Calculated groundwater recharge for all scenarios and sampling locations with indication of vegetation and soil texture.

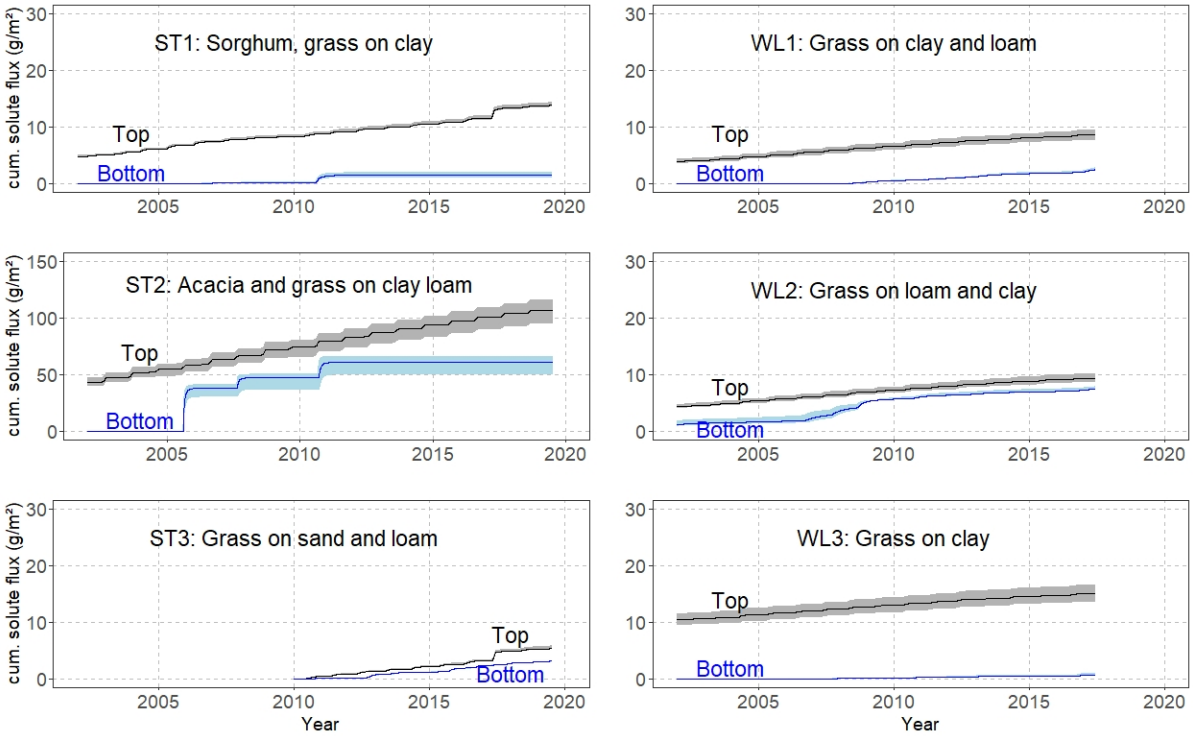

711

712 **Fig. 8: Cumulative solute flux on the upper and lower boundary of the models. The shaded areas represent the standard deviation**
713 **of 100 randomly selected model runs. Note the different y-axis scales between sites.**

714

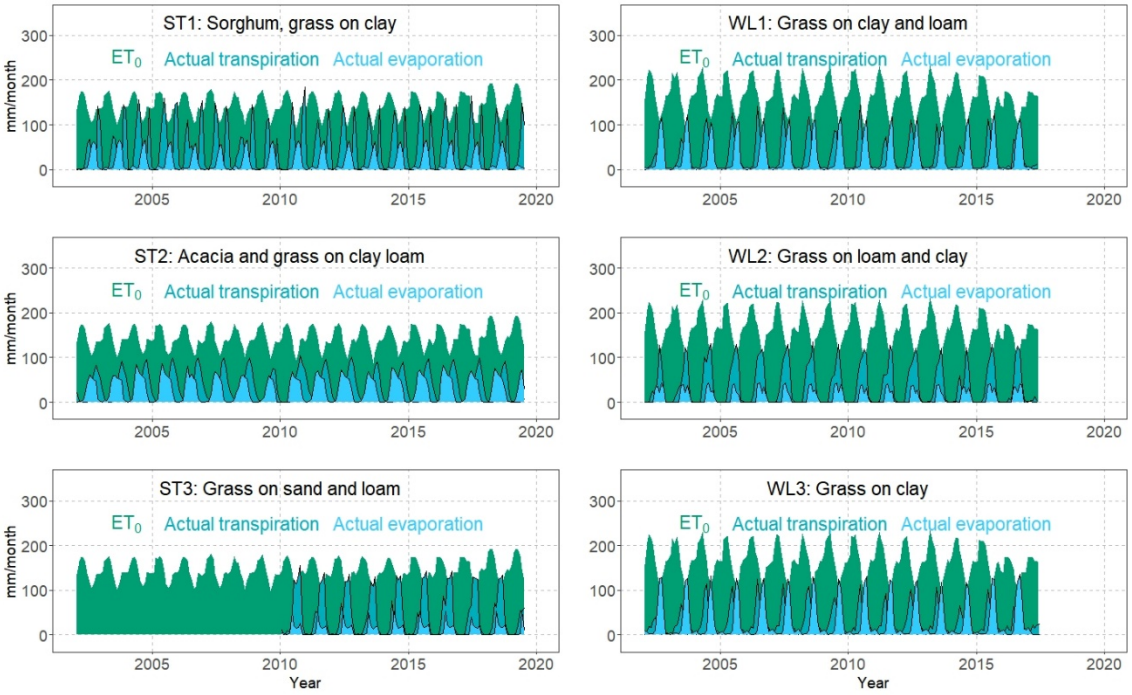

Fig. 9: Reference evapotranspiration from the CRUTS 4 database (NCAR 2017) as well as modelled average actual evaporation and transpiration of 100 randomly selected model runs.

Table 1: Names and geographic coordinates of the sampling locations with average depths to groundwater.

Name	Location	Date of Sampling	Drilling depth (m)	Longitude (°)	Latitude (°)	Elevation (m a.s.l.)	Depth to Groundwater (m)
ST1	Gos Djarat	07-12-2016 11-07-2019	2.35 5.0	19.89644	11.02582	418	11
ST2	Kach Kacha	09-12-2016 16-07-2019	2.0 5.0	20.07473	10.81649	396	16-18
ST3	Gos Djarat	11-12-2016 13-07-2019	2.2 5.0	19.91687	11.00629	418	21
WL1	Katoa	01-06-2017	4.0	15.09235	10.82508	362	4
WL2	Loutou	01-06-2017	3.0	15.37817	10.76805	325	11-12
WL3	Zina	08-06-2017	3.8	14.97363	11.28858	304	3.6

722 **Table 2: Crop evapotranspiration scenarios used with the individual soil profiles.**

Scenario	K_{cb}	K_e	Root depth	Profile
Mean	average	average	average	All profiles
Min	minimum	minimum	average	All profiles
Min-RD	minimum	minimum	minimum	WL1
Mix-1	minimum	average	average	All profiles
Mix-2	average	minimum	average	ST1, WL2, WL3
Mix-3	maximum	average	average	ST3
Max	maximum	maximum	average	All profiles

723

724 **Table 3: Parametrization of water retention and unsaturated hydraulic conductivity functions according the Mualem-van**
725 **Genuchten model after Bayesian model calibration.**

Location	Texture	Depth (m)	θ_r (-)	θ_s (-)	α (m^{-1})	n (-)	k_s (md^{-1})
ST1	Clay	0-1	0.001	0.61±0.01	2.13±0.27	1.164±0.008	0.09±0.14
	Sandy clay	1-2.35	0.04	0.43±0.03	2.63±0.37	1.150±0.011	0.43±0.39
ST2	Sandy clay loam	0-1.4	0.04	0.38±0.02	1.18±0.08	1.36±0.047	0.03±0.16
	Clay	1.4 -2.1	0.07	0.48±0.08	2.66±0.36	1.203±0.052	0.11±0.28
ST3	Loamy fine sand	0-0.8	0.01	0.45±0.08	3.69±0.08	2.332±0.196	2.96±5.72
	Sandy clay loam	0.8-1.5	0.043	0.38±0.07	2.81±0.43	2.210±0.172	2.44±4.19
	Sandy loam	1.5-2.4	0.02	0.43±0.08	3.44±0.51	2.469±0.330	1.66±2.84
	Loamy sand	2.4-2.5	0	0.35±0.06	3.77±0.53	1.980±0.265	2.03±3.11
	Sand	2.5-2.75	0	0.34±0.04	3.73±0.53	2.730±0.372	5.42±8.86
	Loamy sand	2.75-2.84	0	0.35±0.06	3.77±0.53	1.980±0.265	2.03±3.11
	Sand	2.84-2.9	0	0.34±0.04	3.73±0.53	2.730±0.372	5.42±8.86
WL1	Clay	0-0.3	0.065	0.56±0.09	1.37±0.19	1.293±0.092	0.17±0.26
	Sandy clay	0.3-0.9	0.06	0.44±0.07	2.85±0.36	1.416±0.125	0.21±0.38
	Clay	0.9-2.0	0.103	0.42±0.03	1.55±0.21	1.187±0.065	0.19±0.42
	Sandy clay loam	2.0-2.8	0.075	0.49±0.07	2.34±0.33	1.598±0.227	0.13±0.28
	Sandy clay	2.8-3.8	0.081	0.43±0.06	2.60±0.35	1.266±0.134	0.09±0.19
	Sandy clay loam	3.8-4.0	0.071	0.40±0.05	2.69±0.37	1.291±0.137	0.12±0.24
WL2	Sandy clay loam	0-0.2	0.03	0.41±0.07	3.22±0.45	1.502±0.151	0.30±0.57
	Sandy clay	0.2-0.6	0.01	0.37±0.06	2.56±0.39	1.422±0.081	0.09±0.19

	Sandy clay loam	0.6-3.0	0.01	0.37±0.03	1.39±0.19	1.566±0.06	0.10±0.10
	Sandy clay	0-1.4	0.09	0.49±0.09	1.27±0.15	1.470±0.111	0.22±0.14
WL3	Clay	1.4-3.6	0.105	0.53±0.05	2.03±0.29	1.285±0.100	0.17±0.36
	Loamy fine sand	3.6-3.8	0.056	0.39±0.08	2.90±0.45	1.789±0.293	1.23±2.40

Table 4: Average root mean square error (RMSE) and related standard deviation (SD) over all scenarios for water content (Theta) and chloride concentration.

Location, Year	Theta (cm^3 cm^{-3})			Chloride concentration (mg l^{-1})		
	Average observation	Average simulation	Average RMSE	Average observation	Average simulation	Average RMSE
ST1, 2016/2019	0.25/0.22	0.23/0.23	0.06/0.04	30/6	18/22	19/19
ST2, 2016/2019	0.17/0.14	0.16/0.15	0.06/0.04	162/106	132/229	82/116
ST3, 2016/2019	0.06/0.08	0.07/0.06	0.02/0.02	42/10	6/13	58/10
WL1, 2017	0.27	0.27	0.05	31	6	59
WL2, 2017	0.13	0.15	0.02	40	3	117
WL3, 2017	0.31	0.33	0.04	12	13	9

Table 5: Calculated average annual recharge, fraction of recharge on average annual precipitation, standard deviations of recharge across the time-period 2005-2019 and 2005 – 2016 for Salamat and Waza Logone, respectively.

Location	Average annual recharge (mm)	Fraction of average annual precipitation (%)	Standard deviation of annual recharge (mm)
ST1	7	0.9	17
ST2	9	1	29
ST3	93	12	69
WL1	28	4	32
WL2	54	8	46
WL3	6	1	48

737 **Table 6: Calculated average annual evaporation and transpiration and related standard deviations of 100 randomly accepted model**
738 **runs.**

Location	Average annual evaporation (mm)	Standard deviation of evaporation (mm)	Average annual transpiration (mm)	Standard deviations of transpiration (mm)	Average actual evapotranspiration (mm)
ST1	210	9	553	11	763
ST2	366	22	388	27	754
ST3	137	12	552	11	689
WL1	344	20	317	23	661
WL2	146	14	477	28	623
WL3	376	12	305	10	681

739

740

741 Supplement Material

742 **Table S1: Precipitation chloride concentration measured in N'Djamena.**

Sampling Date	Precipitation amount (mm)	Chloride concentration (mg l^{-1})l
16/06/2016	19	1.25
17/06/2016	17	0.82
26/06/2016	20	0.37
12/07/2016	55	0.13
25/07/2016	0.5	0.37
01/08/2016	51	0.29
07/08/2016	13.5	0.17
10/08/2016	23	0.22
24/08/2016	29	0.22
01/09/2016	36	0.20
24/05/2017	1	19.60
30/05/2017	4	3.40
10/06/2017	1	3.24
12/06/2017	12	0.82
21/06/2017	33	1.45
22/06/2017	8	1.12
27/06/2017	11	0.97
30/06/2017	6	0.53
05/07/2017	40	0.39
08/07/2017	30	0.17
17/07/2017	24	0.19
24/07/2017	65	0.15
09/08/2017	55	0.15
15/08/2017	23	0.28
18/08/2017	40	0.17
14/09/2017	29	0.31
25/09/2017	31	0.43
28/05/2018	28	0.91

Sampling Date	Precipitation amount (mm)	Chloride concentration ($mg\ l^{-1}$)l
01/07/2018	60	0.16
07/07/2018	65	0.11
11/07/2018	46	0.16
13/07/2018	43	0.38
30/07/2018	50	0.09
08/08/2018	50	0.13
23/08/2018	80	0.05
07/09/2018	30	0.13
28/05/2019	45	1.89
30/05/2019	30	0.37
22/07/2019	121	0.17
05/08/2019	29	0.09
09/08/2019	45	0.08
27/08/2019	35	0.25
09/09/2019	45	0.46
15/09/2019	43	0.37
01/10/2019	36	0.55
04/10/2019	14	0.46
07/10/2019	20	0.27
04/05/2020	19.3	1.35
05/06/2020	15.9	1.30
09/06/2020	21.4	0.69
15/06/2020	26.5	0.29
19/06/2020	12	0.30
26/06/2020	14.4	0.85
05/07/2020	26.5	0.21
10/07/2020	27.4	0.18
14/07/2020	9.4	0.26
22/07/2020	13.2	0.16
24/07/2020	16.6	0.12
27/07/2020	24.6	0.15

743

744 **Table S2: Soil chloride concentration measured in each of the Salamat profiles. GW (2016): chloride concentration in groundwater**
745 **and year of measurement.**

Site	Depth interval (cm)	Soil chloride concentration ($mg\ l^{-1}$)		Gravimetric water content (%)	
		2016	2019	2016	2019
ST1	0-10	44.75	11.17	0.17	0.31
	10-20	42.14	15.05	0.18	0.18
	20-30	45.55	9.75	0.16	0.16
	30-40	29.40	7.07	0.28	0.20
	40-50	13.53	6.26	0.33	0.21
	50-60	32.15	3.82	0.34	0.23
	60-80	18.54	2.78	0.33	0.24
	80-100	12.26	2.64	0.28	0.24
	100-110	14.55	2.12	0.29	0.25
	110-120	24.89		0.29	
	120-130	29.28	1.72	0.28	0.23
	130-140	18.57		0.27	
	140-150	24.00	1.74	0.25	0.23
	150-160	55.14		0.27	
	160-170	51.84	1.91	0.22	0.23
	170-180	24.65		0.25	
	180-190	40.14	2.25	0.23	0.20
	190-200	28.30		0.22	
	200-210	42.37	15.5	0.22	0.20
	210-220	10.07		0.21	
	220-230	26.71	1.47	0.21	0.18
	230-240	24.25		0.22	
	240-260		1.75		0.16
	260-280		1.42		0.17
	280-300		1.26		0.16
	300-320		1.10		0.16
	320-340		1.76		0.16
	340-360		2.23		0.14

Site	Depth interval (cm)	Soil chloride concentration (mg l^{-1})		Gravimetric water content (%)	
		2016	2019	2016	2019
	360-380		1.14		0.16
	380-400		0.99		0.16
	400-420		1.41		0.16
	420-440		1.35		0.15
	440-460		1.38		0.16
	460-480		1.08		0.17
	480-500		1.02		0.18
GW (2019)	1,100	0.34			
ST2	0-10	269.66	21.07	0.03	0.25
	10-20	115.31	34.16	0.04	0.22
	20-30	82.18	134.77	0.05	0.18
	30-40	60.80	121.60	0.06	0.07
	40-50	98.79	40.65	0.09	0.08
	50-60	194.90	24.57	0.09	0.09
	60-70	210.85	28.27	0.06	0.08
	70-80	46.03		0.06	
	80-90	30.47	69.27	0.08	0.09
	90-100	36.89		0.08	
	100-110	37.52	160.93	0.08	0.10
	110-120	144.63		0.05	
	120-130	258.28	202.94	0.07	0.15
	130-140	233.81		0.17	
	140-150	304.90	206.61	0.16	0.20
	150-160	368.07		0.12	
	160-170	207.07	186.64	0.12	0.18
	170-180	158.34		0.13	
	180-190	191.84	146.81	0.12	0.14
	190-200	201.77		0.12	
	200-220		117.61		0.14
	220-240		82.31		0.14

Site	Depth interval (cm)	Soil chloride concentration (mg l^{-1})		Gravimetric water content (%)	
		2016	2019	2016	2019
	240-260		65.10		0.13
	260-280		48.25		0.13
	280-300		32.34		0.12
	300-320		25.89		0.12
	320-340		27.25		0.12
	340-360		26.81		0.12
	360-380		41.14		0.13
	380-400		49.37		0.14
	400-420		53.52		0.14
	420-440		56.65		0.14
	440-460		55.76		0.10
	460-480		101.40		0.01
	480-500		149.20		0.01
GW (2016)	1,700	1.39			
ST3	0-10	172.79	9.27	0.01	0.09
	10-20	73.81	15.44	0.02	0.08
	20-30	45.54	18.40	0.02	0.07
	30-40	37.08	8.65	0.03	0.06
	40-50	25.53	13.64	0.04	0.05
	50-60	10.71	6.38	0.08	0.05
	60-70	41.26		0.05	
	70-80	23.95	7.62	0.06	0.05
	80-90	30.15		0.07	
	90-100	15.67	6.12	0.08	0.07
	100-110	11.67		0.09	
	110-120	21.20	4.06	0.09	0.07
	120-130	54.53		0.10	
	130-140	19.90	6.48	0.10	0.06
	140-150	12.27		0.10	
	150-160	13.14	7.03	0.07	0.04

Site	Depth interval (cm)	Soil chloride concentration (mg l^{-1})		Gravimetric water content (%)	
		2016	2019	2016	2019
	160-170	16.54		0.05	
	170-180	15.62	11.41	0.04	0.04
	180-190	15.96		0.05	
	190-200	14.55	10.19	0.07	0.03
	200-210	7.40		0.08	
	210-220	14.77	8.93	0.10	0.08
	220-230	12.77		0.12	
	230-240	22.53	15.25	0.07	0.03
	240-250	101.22		0.03	
	250-260	80.82	7.08	0.03	0.03
	260-270	171.44		0.02	
	270-280	66.03	18.41	0.03	0.02
	280-300	88.52	11.64	0.02	0.02
	300-320		28.13		0.02
	320-340		24.83		0.01
	340-360		37.71		0.01
	360-380		30.59		0.02
	380-400		29.21		0.02
	400-420		32.63		0.02
	420-440		36.39		0.02
	440-460				
	460-480		39.34		0.02
	480-500		39.51		0.02
GW (2016)	2,100	4.10			

Table S3: Soil chloride concentration measured in each of the Waza Logone profiles in 2017. GW (2016): chloride concentration in groundwater and year of measurement.

Site	Depth interval (cm)	Soil chloride concentration (mg l^{-1})	Gravimetric water content (%)
WL1	0-10	246.74	0.12
	10-20	142.34	0.13
	20-30	39.42	0.12
	30-40	17.99	0.11
	40-50	18.03	0.07
	50-60	26.61	0.08
	60-70	9.44	0.11
	70-80	4.36	0.13
	80-90	8.31	0.15
	90-100	11.22	0.18
	100-120	7.33	0.16
	120-140	4.26	0.15
	140-160	3.65	0.16
	160-180	12.24	0.18
	180-200	3.11	0.19
	200-220	3.00	0.14
	220-240	7.18	0.11
	240-260	22.38	0.15
	260-280	18.40	0.14
	280-300	17.46	0.16
	300-320	16.14	0.17
	320-340	46.94	0.18
	340-360	24.16	0.17
	360-380	75.87	0.15
	380-400	6.86	0.15
GW (2017)	400	0.23	
WL2	0-10	446.21	0.03
	10-20	269.74	0.02
	20-30	106.04	0.04
	30-40	35.22	0.06

Site	Depth interval (cm)	Soil chloride concentration (mg l^{-1})	Gravimetric water content (%)
	40-50	44.11	0.06
	50-60	19.47	0.07
	60-80	18.40	0.08
	80-100	17.55	0.07
	100-120	15.36	0.06
	120-140	12.12	0.07
	140-160	101.76	0.07
	160-180	15.07	0.08
	180-200	5.86	0.09
	200-220	4.90	0.09
	220-240	3.85	0.09
	240-260	2.69	0.09
	260-280	2.73	0.10
	280-300	4.87	0.10
GW (2014)	1,200	0.90	
	0-10	157.35	0.06
	10-20	50.59	0.09
	20-30	13.32	0.11
	30-40	32.41	0.11
	40-50	14.77	0.11
	50-60	9.02	0.12
	60-80	8.85	0.12
	80-100	10.27	0.13
WL3	100-120	6.84	0.13
	120-140	6.28	0.13
	140-160	5.59	0.15
	160-180	7.63	0.20
	180-200	11.47	0.21
	200-220	4.83	0.19
	220-240	5.30	0.19
	240-260	4.74	0.21

Site	Depth interval (cm)	Soil chloride concentration (mg l^{-1})	Gravimetric water content (%)
	260-280	4.98	0.22
	280-300	9.54	0.23
	300-320	10.24	0.21
	320-340	9.75	0.22
	340-360	9.25	0.23
	360-380	21.78	0.17
GW (2017)	360	1.51	

753

754 **Table S4: Site-specific estimated monthly variation of ground cover including grass, crops, and flooding periods with ranges of**
755 **monthly basal crop coefficient (Kcb), soil water evaporation coefficient (Ke), and root depth used in the scenarios.**

Location	Month	Vegetation	Kcb	Ke	Root depth (m)
ST1	Jan	Sorghum	1.01 – 0.86	0.12	1.5 – 2.5
	Feb	Sorghum	0.35 – 0.35	0.48	1.5 – 2.5
	Mar	Bare soil	0.0	0.47 – 0.68	0.0
	Apr	Bare soil	0.0	0.27 – 0.41	0.0
	May	Grass	0.6 – 0.4	0.1 – 0.12	0.1 – 0.5
	June	Grass	0.85 – 0.6	0.05	0.2 – 0.7
	July	Grass	1.03 – 0.83	0.12	0.2– 0.7
	Aug	Flooded	0.3 – 0.2	0.9 – 1.0	0.2 – 0.7
	Sep	Flooded	0.0	1.08	0.0
	Oct	Flooded	0.0	1.08	0.0
	Nov	Sorghum	0.2 – 0.1	0.66	0.5 – 1.5
	Dec	Sorghum	1.01 – 0.86	0.12	1.5 – 2.5
ST2	Jan	Tree (Acacia)	0.5 – 0.8	0.2 – 0.34	Time invariant root distribution
	Feb	Tree	0.2 – 0.6	0.17 – 0.39	
	Mar	Tree	0.1 – 0.3	0.07 – 0.37	
	Apr	Tree	0.1 – 0.3	0.02 – 0.17	
	May	Tree, Grass	0.1 – 0.3	0.5	
	June	Tree, Grass	0.3 – 0.4	0.5	
	July	Tree, Grass	0.3 – 0.4	0.5	
	Aug	Tree, flooded	0.6 – 0.8	0.25	

Location	Month	Vegetation	Kcb	Ke	Root depth (m)
	Sep	Tree, flooded	0.7 – 1.05	0.25	
	Oct	Tree, flooded	0.7 – 1.05	0.25	
	Nov	Tree, Grass	0.7 – 0.9	0.25	
	Dec	Tree	0.5 – 0.8	0.32 – 0.37	
ST3	Jan	Grass	0.05 – 0.1	0.13 – 0.39	0.1
	Feb	Dry Grass	0.0 – 0.05	0.04 – 0.13	0.1
	Mar	Dry Grass	0.0 – 0.05	0.0	0.1 – 0.2
	Apr	Grass	0.1 – 0.3	0.0	0.2 – 0.3
	May	Green grass	0.6	0.0	0.2 – 0.3
	June	Green grass	0.65 – 0.85	0.34 – 0.54	0.2 – 0.4
	July	Green grass	0.73 – 1.03	0.16 - 0.24	0.2 – 0.4
	Aug	Green grass	0.83 – 1.03	0.09 - 0.22	0.2 – 0.4
	Sep	Green grass	0.83 – 0.98	0.14 - 0.22	0.2 – 0.4
	Oct	Green grass	0.78 – 0.93	0.19 - 0.22	0.2 – 0.3
	Nov	Green grass	0.4 – 0.6	0.51	0.1 – 0.3
	Dec	Grass	0.05 – 0.1	0.4 – 0.67	0.1
WL1	Jan	Bare soil	0.0 – 0.1	0.29 – 0.63	0.0 – 0.2
	Feb	Bare soil	0.0 – 0.1	0.16 – 0.42	0.0 – 0.2
	Mar	Bare soil	0.10	0.07 – 0.25	0.05 – 0.3
	Apr	Grass	0.30 – 0.4	0.03 – 0.1	0.1 – 0.3
	May	Grass	0.40	0.02 – 0.08	0.1 – 0.5
	June	Grass	0.70 – 0.9	0.01 – 0.02	0.1 – 0.5
	July	Grass	0.89 – 1.09	0.13	0.1 – 0.5
	Aug	Flooded	0.1 – 0.2	0.92 - 1.01	0.1 – 0.4
	Sep	Flooded	0.1 – 0.2	0.92 - 1.01	0.0 – 0.1
	Oct	Flooded	0.1 – 0.2	0.92 - 1.01	0.0 – 0.1
	Nov	Grass	0.2 – 0.5	0.58 – 0.62	0.05 – 0.2
	Dec	Grass	0.2 – 0.4	0.37 – 0.57	0.05 – 0.2
WL2	Jan	Bare soil	0.0 – 0.1	0.11 – 0.57	0.0 – 0.1
	Feb	Bare soil	0.0 – 0.1	0.03 – 0.24	0.0 – 0.1
	Mar	Bare soil	0.1 – 0.2	0.0 – 0.07	0.05 – 0.1
	Apr	Grass	0.2 – 0.3	0.0 – 0.02	0.05 – 0.2

Location	Month	Vegetation	Kcb	Ke	Root depth (m)
	May	Grass	0.4 – 0.4	0.0 – 0.01	0.15 – 0.3
	June	Grass	0.45 – 0.6	0.0	0.15 – 0.3
	July	Grass	0.5 – 0.7	0.55 - 0.75	0.15 – 0.3
	Aug	Grass	0.45 – 1.0	0.12 - 0.22	0.1 – 0.3
	Sep	Flooded	0.3 – 1.0	0.12 - 0.22	0.1 – 0.3
	Oct	Grass	0.2 – 0.7	0.42 - 0.67	0.15 – 0.2
	Nov	Grass	0.1 – 0.2	0.77	0.15 – 0.2
	Dec	Grass	0.0 – 0.1	0.32 – 0.9	0.05 – 0.1
WL3	Jan	Bare soil	0.0 – 0.1	0.28 – 0.6	0.1 – 0.2
	Feb	Bare soil	0.0 – 0.1	0.15 – 0.4	0.1 – 0.2
	Mar	Bare soil	0.1 – 0.1	0.06 – 0.23	0.1 – 0.5
	Apr	Grass	0.2 – 0.4	0.03 – 0.09	0.2 – 0.5
	May	Grass	0.4	0.01 – 0.08	0.2 – 0.6
	June	Grass	0.4 – 0.9	0.01 - 0.01	0.2 – 0.6
	July	Grass	0.79 – 1.09	0.13	0.2 – 0.6
	Aug	Flooded	0.1 – 0.2	0.92 - 1.01	0.2 – 0.6
	Sep	Flooded	0.0 – 0.1	1.01	0.2 – 0.6
	Oct	Flooded	0.0 – 0.1	1.01	0.2 – 0.5
	Nov	Grass	0.2 – 0.5	0.58	0.1 – 0.5
	Dec	Grass	0.1 – 0.4	0.1 - 0.41	0.1 – 0.2

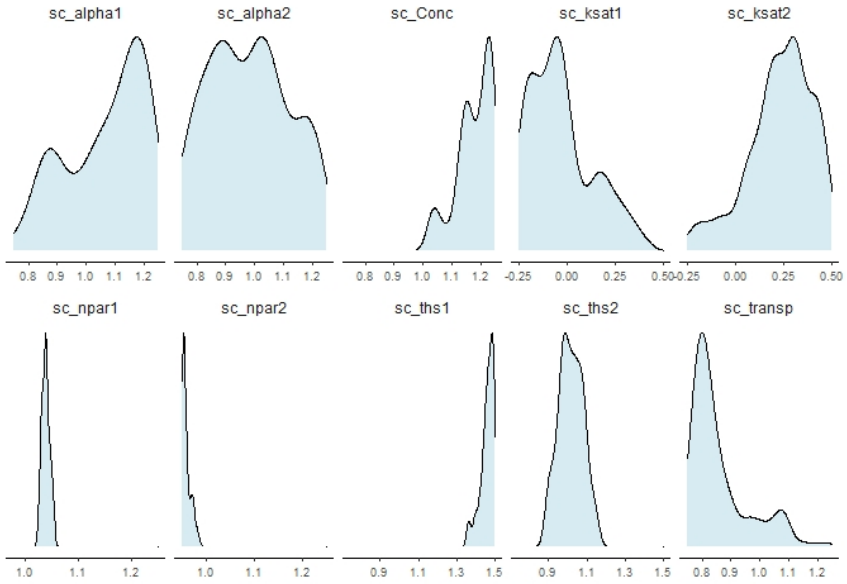

Fig. S1: posterior density distributions of the scaling factors used in the calibration of model ST1. Numbers indicate the individual model layers. Range of x-axes corresponds to prior distribution (parameter alpha of the Mualem-van Genuchten equation: sc_alpha1. sc_alpha2: alpha; sc_Conc: input chloride conctentration; sc_ksat1. sc_ksat2: saturated hydraulic conductivity; sc_npart1. sc_npart2: parameter n of the Mualem-van Genuchten equation ; sc_ths1. sc_ths2: saturated water content; sc_transp: transpiration fraction in the evapotranspiration; 1: upper layer; 2: lower layer).

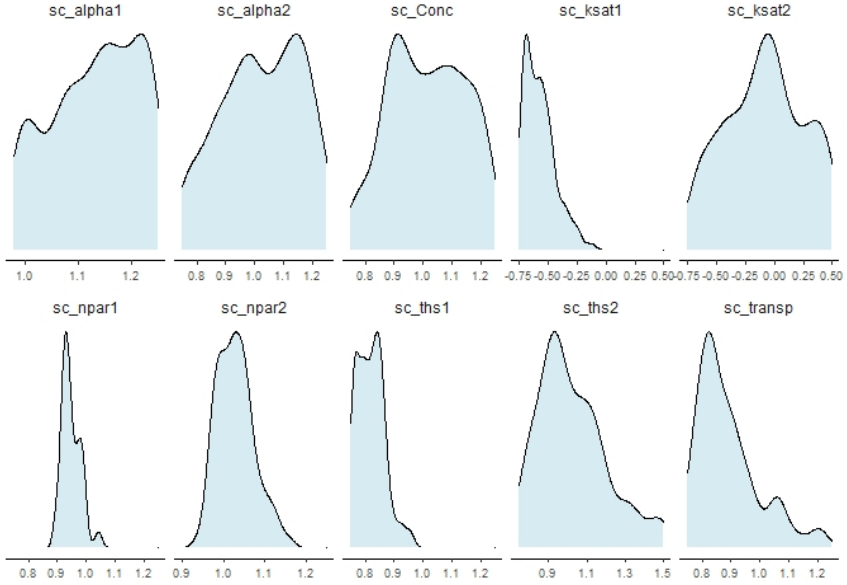

Fig. S2: posterior density distributions of the scaling factors used in the calibration of model ST2. Numbers indicate the individual model layers. Range of x-axes corresponds to prior distribution.

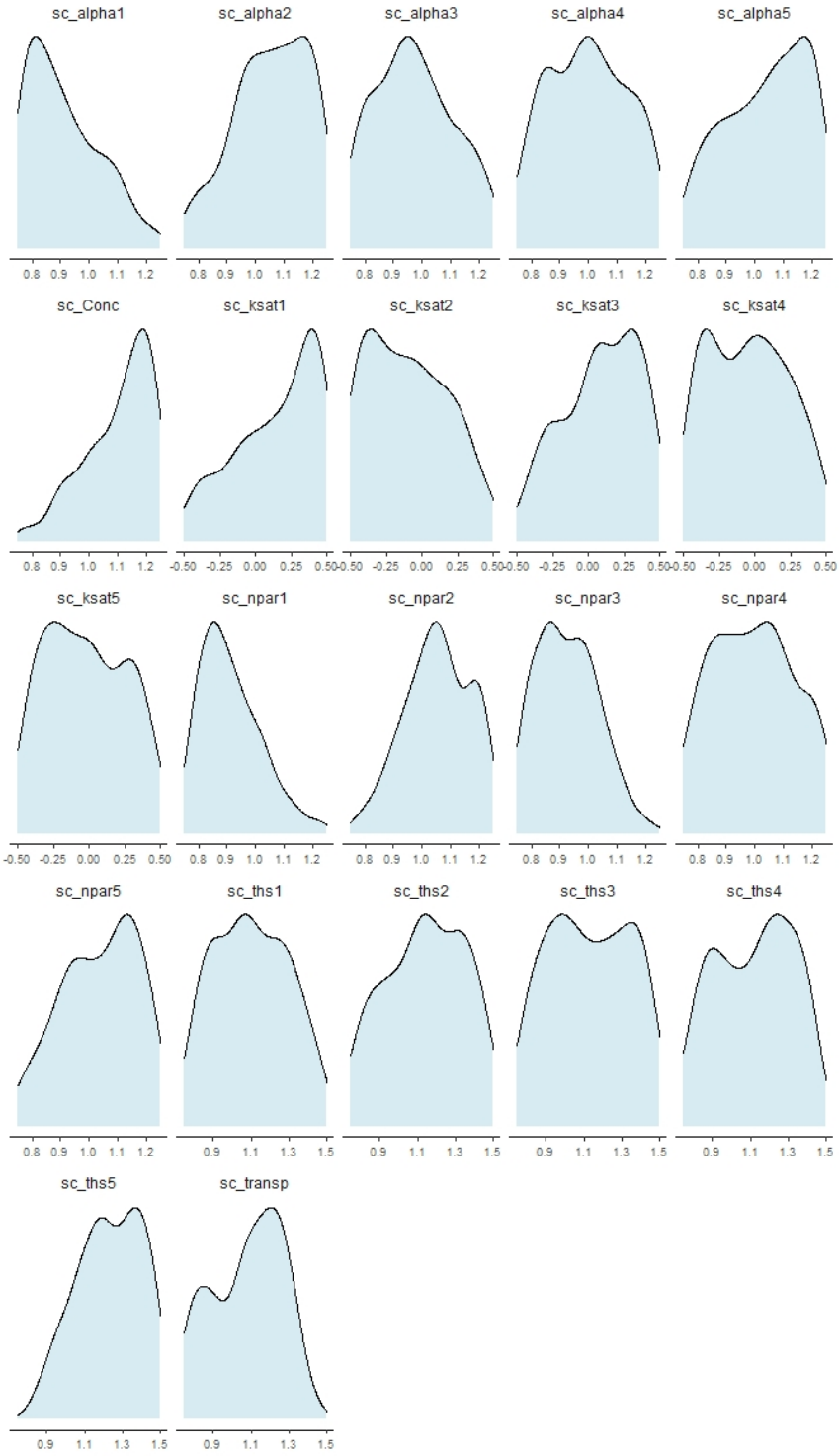

Fig. S3: posterior density distributions of the scaling factors used in the calibration of model ST3. Numbers indicate the individual model layers. Range of x-axes corresponds to prior distribution.

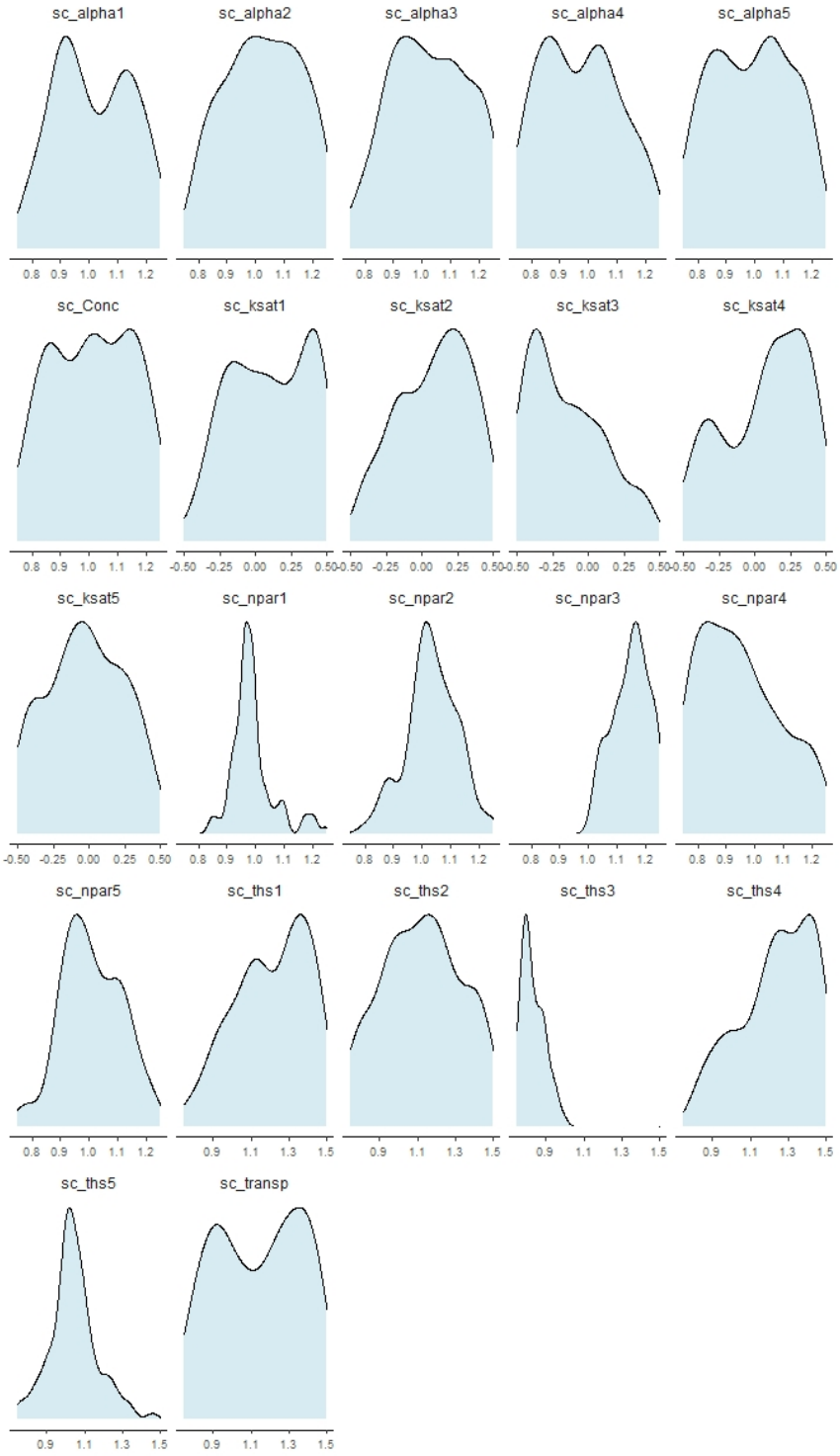

Fig. S4: posterior density distributions of the scaling factors used in the calibration of model WL1. Numbers indicate the individual model layers. Range of x-axes corresponds to prior distribution.

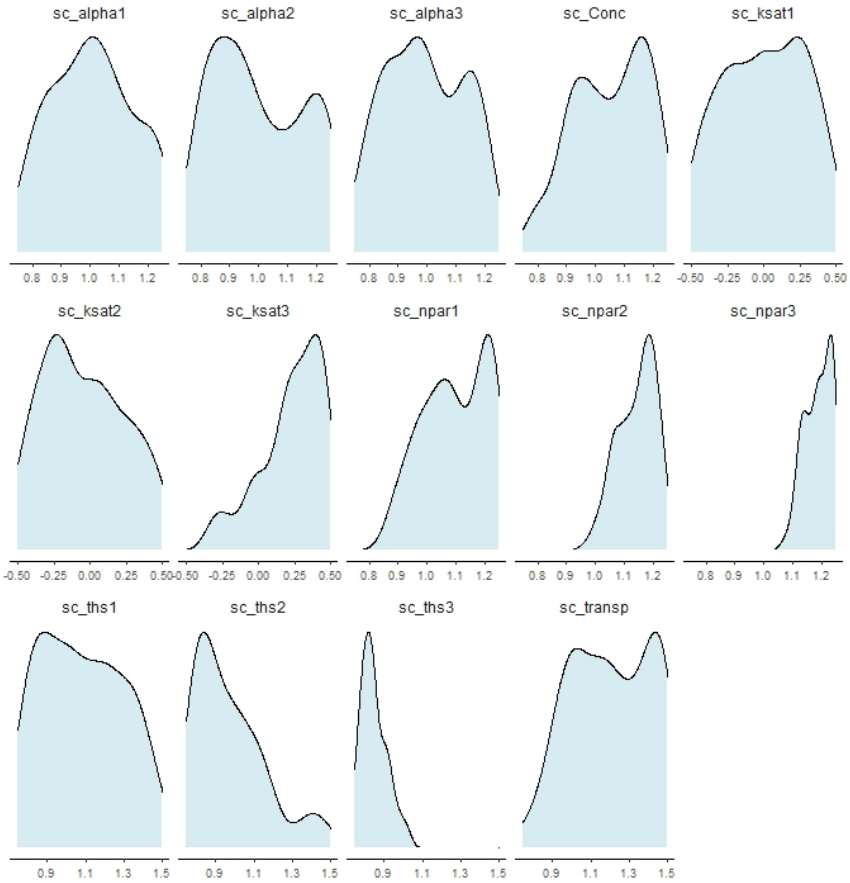

773

774 **Fig. S5: posterior density distributions of the scaling factors used in the calibration of model WL2. Numbers indicate the individual**
775 **model layers. Range of x-axes corresponds to prior distribution.**

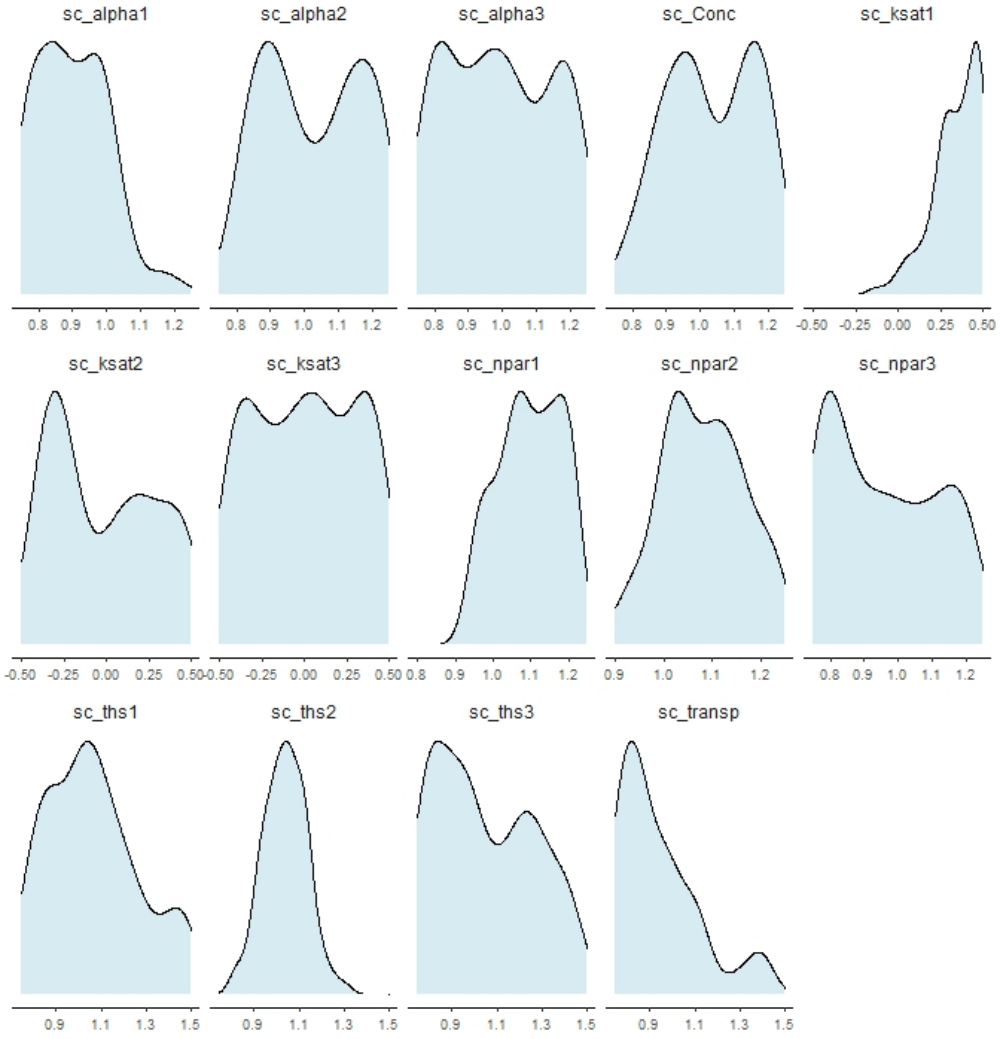

Fig. S6: posterior density distributions of the scaling factors used in the calibration of model WL3. Numbers indicate the individual model layers. Range of x-axes corresponds to prior distribution.